17. Lattice Quantum Chromodynamics

Revised August 2025 by C. Davies (U. Glasgow), S. Hashimoto (KEK), S. Meinel (U. Arizona), and S.R. Sharpe (U. Washington); originally written September 2011 by S. Hashimoto, J. Laiho (Syracuse U.), and S.R. Sharpe

Many physical processes considered in the Review of Particle Properties (RPP) involve hadrons. The properties of hadrons—which are composed of quarks and gluons—are governed primarily by Quantum Chromodynamics (QCD) (with small corrections from Quantum Electrodynamics [QED]). Theoretical calculations of these properties require non-perturbative methods, and Lattice Quantum Chromodynamics (LQCD) is a tool to carry out such calculations. It has been successfully applied to many properties of hadrons. Most important for the RPP are the calculation of electroweak decay constants and form factors, which are needed to extract Cabbibo-Kobayashi-Maskawa (CKM) matrix elements when combined with the corresponding experimental measurements. LQCD has also been used to determine other fundamental parameters of the standard model, in particular the strong gauge coupling and quark masses, as well as to predict hadronic contributions to the anomalous magnetic moment of the muon, $g-2$.

This review describes the theoretical foundations of LQCD and sketches the methods used to calculate the quantities relevant for the RPP. It also describes the various sources of error that must be controlled in a LQCD calculation. Results for hadronic quantities are found in the corresponding dedicated reviews.

17.1 Lattice regularization of QCD

Gauge theories form the building blocks of the Standard Model. While the SU(2) and U(1) parts have weak couplings and can be studied accurately with perturbative methods, the SU(3) component—QCD—is only amenable to a perturbative treatment at high energies. The growth of the gauge coupling in the infrared—the flip-side of asymptotic freedom—requires the use of non-perturbative methods to determine the low energy properties of QCD. Lattice gauge theory, proposed by K. Wilson in 1974 [1], provides such a method, for it gives a non-perturbative definition of vector-like gauge field theories such as QCD. In lattice regularized QCD—commonly called lattice QCD or LQCD—Euclidean space-time is discretized, usually on a hypercubic lattice with lattice spacing a, with quark fields placed on sites and gauge fields on the links between sites. The lattice spacing plays the role of the ultraviolet regulator, rendering the quantum field theory finite. The continuum theory is recovered by taking the limit of vanishing lattice spacing, which can be reached by tuning the bare gauge coupling to zero according to the renormalization group.

Unlike dimensional regularization, which is commonly used in continuum QCD calculations, the definition of LQCD does not rely on the perturbative expansion. Indeed, LQCD allows non-perturbative calculations by numerical evaluation of the path integral that defines the theory.

Practical LQCD calculations are limited by the availability of computational resources and the efficiency of algorithms. Because of this, LQCD results come with both statistical and systematic errors, the former arising from the use of Monte-Carlo integration, the latter, for example, from the use of non-zero values of a. There are also different ways in which the QCD action can be discretized, and all must give consistent results in the continuum limit, $a \to 0$. It is the purpose of this review to provide an outline of the methods of LQCD, with particular focus on applications to particle physics, and an overview of the various sources of error. This should allow the reader to better understand the LQCD results that are presented in other reviews, primarily those on "Quark Masses," "Quark Model," "Quantum Chromodynamics," "CKM quark-mixing matrix," "V_{ud}, V_{us}, Cabibbo angle and CKM Unitarity," "Leptonic Decays of Charged Pseudoscalar Mesons," "B^0-$\bar{B}^0$ Mixing," and "Semileptonic b-Hadron Decays, Determination of V_{cb} and V_{ub}." For more extensive explanations the reader should consult the available textbooks or lecture notes, the most up-to-date of which are Refs. [2–4].

17.1.1 *Gauge invariance, gluon fields and the gluon action*

A key feature of the lattice formulation of QCD is that it preserves gauge invariance. This is in contrast to perturbative calculations, where gauge fixing is an essential step. The preservation of gauge invariance leads to considerable simplifications, e.g., restricting the form of operators that can mix under renormalization.

The gauge transformations of lattice quark fields are just as in the continuum: $q(x) \longrightarrow V(x)q(x)$ and $\bar{q}(x) \longrightarrow \bar{q}(x)V^\dagger(x)$, with $V(x)$ an arbitrary element of SU(3). The only difference is that the Euclidean space-time positions x are restricted to lie on the sites of the lattice, i.e. $x = a(n_1, n_2, n_3, n_4)$ for a hypercubic lattice, with the n_j being integers. Quark bilinears involving different lattice points can be made gauge invariant by introducing the gluon field $U_\mu(x)$. For example, for adjacent points the bilinear is $\bar{q}(x)U_\mu(x)q(x+a\hat{\mu})$, with $\hat{\mu}$ the unit vector in the μ'th direction. (This form is used in the construction of the lattice covariant derivative.) This is illustrated in Fig. 17.1. The gluon field (or "gauge link") is an element of the group, SU(3), in contrast to the continuum field A_μ which takes values in the Lie algebra. The bilinear is invariant if U_μ transforms as $U_\mu(x) \to V(x)U_\mu(x)V^\dagger(x+a\hat{\mu})$. The lattice gluon field is naturally associated with the link joining x and $x+a\hat{\mu}$, and corresponds in the continuum to a Wilson line connecting these two points, $\mathrm{P}\exp(i\int_x^{x+a\hat{\mu}} dx_\mu A_\mu^{\mathrm{cont}}(x))$ (where P indicates a path-ordered integral, and the superscript on A_μ indicates that it is a continuum field). The trace of a product of the $U_\mu(x)$

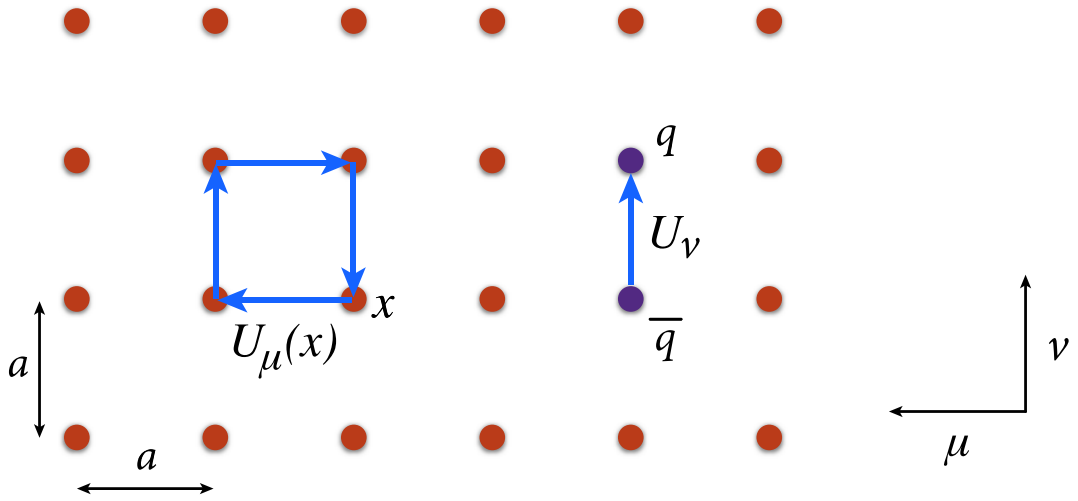

Figure 17.1: Sketch of a two-dimensional slice through the $\mu-\nu$ plane of a lattice, showing gluon fields lying on links and forming either the plaquette product appearing in the gauge action or a component of the covariant derivative connecting quark and antiquark fields.

around any closed loop is easily seen to be gauge invariant and is the lattice version of a Wilson loop.

The simplest possible gauge action, usually called the Wilson gauge action, is given by the product of gauge links around elementary plaquettes:

$$S_g = \beta \sum_{x,\mu<\nu} [1 - \frac{1}{3}\mathrm{ReTr}[U_\mu(x)U_\nu(x+a\hat{\mu})U_\mu^\dagger(x+a\hat{\nu})U_\nu^\dagger(x)]] \,. \tag{17.1}$$

This is illustrated in Fig. 17.1. For small a, assuming that the fields are slowly varying, one can expand the action in powers of a using $U_\mu(x) = \exp(iaA_\mu(x))$. Keeping only the leading non-vanishing term, and replacing the sum with an integral, one finds the continuum form,

$$\begin{aligned} S_g &\longrightarrow \int d^4x \frac{1}{4g_{\rm lat}^2}\mathrm{Tr}[F_{\mu\nu}^2(x)] \,, \\ &(F_{\mu\nu} = \partial_\mu A_\nu - \partial_\nu A_\mu + i[A_\mu, A_\nu]) \end{aligned} \tag{17.2}$$

as long as one chooses $\beta = 6/g_{\rm lat}^2$ for the lattice coupling. In this expression, $g_{\rm lat}$ is the bare gauge coupling in the lattice scheme, which can be related (by combining continuum and lattice perturbation theory) to a more conventional gauge coupling such as that in the $\overline{\rm MS}$ scheme (see Sec. 17.3.5 below).

In practice, the lattice spacing a is non-zero, leading to discretization errors. In particular, the lattice breaks Euclidean rotational invariance (which is the Euclidean version of Lorentz invariance) down to a discrete hypercubic subgroup. One wants to reduce discretization errors as much as possible. A very useful tool for understanding and then reducing discretization errors is the Symanzik effective action: the interactions of quarks and gluons with momenta low compared to the lattice cutoff ($|p| \ll 1/a$) are described by a continuum action consisting of the standard continuum terms (e.g., the gauge action given in Eq. (17.2)) augmented by higher dimensional operators suppressed by powers of a [5]. For the Wilson lattice gauge action, the leading corrections to the continuum terms come in at $\mathcal{O}(a^2)$. They take the form $\sum_j a^2 c_j O_6^{(j)}$, with the sum running over all dimension-six operators $O_6^{(j)}$ allowed by the *lattice* symmetries, and c_j unknown coefficients. Some of these

operators violate Euclidean rotational invariance, and all of them lead to discretization errors of the form $a^2\Lambda^2$ (up to $\log(a)$ corrections that will be discussed below), where Λ is a typical momentum scale for the quantity being calculated. These errors can, however, be reduced by adding corresponding operators to the lattice action and tuning their coefficients to eliminate the dimension-six operators in the effective action to a given order in perturbation theory or even non-perturbatively. This is the idea of the Symanzik improvement program [5]. In the case of the gauge action, one adds Wilson loops involving six gauge links (as opposed to the four links needed for the original plaquette action, Eq. (17.1)) to define the $\mathcal{O}(a^2)$ improved (or "Symanzik") action [6]. In practical implementations, the improvement is either at tree-level (so that residual errors are proportional to $\alpha_s a^2$, where the coupling is evaluated at a scale $\sim 1/a$ giving the $\log(a)$ dependence mentioned above)), or at one-loop order (errors proportional to $\alpha_s^2 a^2$). Another popular choice is motivated by studies of renormalization group (RG) flow. It has the same terms as the $\mathcal{O}(a^2)$ improved action but with different coefficients, and is called the RG-improved or "Iwasaki" action [7].

17.1.2 *Lattice fermions*

Discretizing the fermion action turns out to involve subtle issues, and the range of actions being used is more extensive than for gauge fields. Recall that the continuum fermion action is $S_f = \int d^4x\, \bar{q}[D_\mu\gamma_\mu + m_q]q$, where $D_\mu = \partial_\mu + iA_\mu$ is the gauge-covariant derivative. The simplest discretization replaces the derivative with a symmetric difference:

$$D_\mu q(x) \longrightarrow \frac{1}{2a}[U_\mu(x)q(x+a\hat{\mu}) - U_\mu(x-a\hat{\mu})^\dagger q(x-a\hat{\mu})]\,. \tag{17.3}$$

The factors of U_μ ensure that $D_\mu q(x)$ transforms under gauge transformations in the same way as $q(x)$, so that the discretized version of $\bar{q}(x)\gamma_\mu D_\mu q(x)$ is gauge invariant. The choice in Eq. (17.3) leads to the so-called naive fermion action. This, however, suffers from the fermion doubling problem—in d dimensions it describes 2^d equivalent fermion fields in the continuum limit. The appearance of the extra "doubler" fermions is related to the deeper theoretical problem of formulating chirally symmetric fermions on the lattice. This is encapsulated by the Nielsen-Ninomiya theorem [8]: one cannot define lattice fermions having exact chiral symmetry of the standard form $\delta q = \epsilon\gamma_5 q$, $\delta\bar{q} = \epsilon\bar{q}\gamma_5$ (ϵ is infinitesimal) without producing doublers. Naive lattice fermions do have chiral symmetry but at the cost of introducing 15 unwanted doublers (for $d = 4$).

There are a number of different strategies for dealing with the doubling problem, each with their own theoretical and computational advantages and disadvantages. Wilson fermions [1] add a term proportional to $a\bar{q}\Delta q$ to the fermion action (the "Wilson term"—in which Δ is a covariant lattice Laplacian). This gives a mass of $\mathcal{O}(1/a)$ to the doublers, so that they decouple in the continuum limit. The Wilson term, however, violates chiral symmetry at non-zero lattice spacing, and introduces discretization errors linear in a. A commonly used variant that eliminates the $\mathcal{O}(a)$ discretization error is the $\mathcal{O}(a)$-improved Wilson (or "clover") action [9]. In this application of Symanzik improvement, methods have been developed to remove $\mathcal{O}(a)$ terms non-perturbatively using auxiliary simulations to tune parameters [10]. Such "non-perturbative improvement" is of great practical importance as it brings the discretization error from the fermion action down to the same level as that from the Wilson gauge action.

The advantages of Wilson fermions are their theoretical simplicity and relatively low computational cost. Their main disadvantage is the lack of chiral symmetry, which makes them difficult to use in cases where mixing with wrong chirality operators can occur, particularly if this involves divergences proportional to powers of $1/a$. A related problem is the presence of potential numerical instabilities due to spurious near-zero modes of the lattice Dirac operator. There are, however, studies that successfully ameliorate the problems due to the lack of chiral symmetry and increase the range of quantities for which Wilson fermions can be used (see, e.g., Refs. [11–13]).

Twisted-mass fermions [14] are a variant of Wilson fermions in which two flavors are treated together with an isospin-breaking mass term (the "twisted mass" term). The main advantage of this approach is that all errors linear in a are automatically removed (without the need for tuning of parameters) by a clever choice of twisted mass and operators [15]. A disadvantage is the presence of isospin breaking effects (such as a splitting between charged and neutral pion masses even when up and down quarks are degenerate), which, however, vanish as $a^2\Lambda^2$ in the continuum limit. Strange and charm quarks can be added as a second pair, with a term added to split their masses [16,17].

Staggered fermions are a reduced version of naive fermions in which there is only a single fermion Dirac component on each lattice site, with the full Dirac structure built up from neighboring sites [18]. They have the advantages of being faster to simulate than Wilson-like fermions, of preserving some chiral symmetry, and of having discretization errors of $\mathcal{O}(a^2)$. Their disadvantage is that they retain some of the doublers (3 for $d = 4$). The action thus describes four degenerate fermions in the continuum limit. These are usually called "tastes", to distinguish them from physical flavors, and the corresponding SU(4) symmetry is referred to as the "taste symmetry". The preserved chiral symmetry in this formulation has non-singlet taste. Practical applications usually introduce one staggered fermion for each physical flavor, and remove contributions from the unwanted tastes by taking the fourth-root of the fermion determinant appearing in the path integral. The validity of this "rooting" procedure is not obvious because taste symmetry is violated for non-zero lattice spacing. Theoretical arguments, supported by numerical evidence, suggest that the procedure is valid as long as one takes the continuum limit before approaching the light quark mass region [19]. Additional issues arise for the valence quarks (those appearing in quark propagators, as described in Sec. 17.2 below), where rooting is not possible, and one must ignore the extra tastes, or account for them by including appropriate factors [20], which can be nontrivial in applications involving baryons [21].

Just as for Wilson fermions, the staggered action can be improved, so as to reduce discretization errors. The Asqtad (a-squared tadpole improved) action [22] was used until recently in many large scale simulations [23]. More recent calculations use the HISQ (highly improved staggered quark) action, introduced in Ref. [24]. At tree-level it removes both $\mathcal{O}(a^2)$ errors and, to lowest order in the quark speed v/c, $\mathcal{O}([am]^4)$ errors. It also substantially reduces effects caused by taste-symmetry breaking. This makes it attractive not only for light quarks, but means that it is also quite accurate for heavy quarks because it suppresses $(am)^n$ errors. It is being used to directly simulate charm quarks and to approach direct simulations of bottom quarks (for early studies, see, e.g., [25–27]).

There is an important class of lattice fermions, "Ginsparg-Wilson fermions," that possess a continuum-like chiral symmetry without introducing unwanted doublers. The lattice Dirac operator D for these fermions satisfies the Ginsparg-Wilson relation $D\gamma_5 + \gamma_5 D = aD\gamma_5 D$ [28]. In the continuum, the right-hand-side vanishes, leading to chiral symmetry. On the lattice, it is non-vanishing, but with a particular form (with two factors of D) that restricts the violations of chiral symmetry in Ward-Takahashi identities to short-distance terms that do not contribute to physical matrix elements [29]. In fact, one can define a modified chiral transformation on the lattice (by including dependence on the gauge fields) such that Ginsparg-Wilson fermions have an exact chiral symmetry for on-shell quantities [30]. The net result is that such fermions essentially have the same properties under chiral transformations as do continuum fermions, including the index theorem [29]. Their leading discretization errors are of $\mathcal{O}(a^2)$.

Two types of Ginsparg-Wilson fermions are currently being used in large-scale numerical simulations. The first is Domain-wall fermions (DWF). These are defined on a five-dimensional space, in which the fifth dimension is fictitious [31]. The action is chosen so that the low-lying modes are chiral, with left- and right-handed modes localized on opposite four-dimensional surfaces. For an infinite fifth dimension, these fermions satisfy the Ginsparg-Wilson relation. In practice, the fifth

dimension is kept finite, and there remains a small, controllable violation of chiral symmetry. The second type is Overlap fermions. These appeared from a completely different context and have an explicit form that exactly satisfies the Ginsparg-Wilson relation [32]. Their numerical implementation requires an approximation of the matrix sign function of a Wilson-like fermion operator, and various approaches are being used. In fact, it is possible to rewrite these approximations in terms of a five-dimensional formulation, showing that the DWF and Overlap approaches are essentially equivalent [33,34]. Numerically, the five-dimensional approach appears to be more computationally efficient.

The various lattice fermion formulations are often combined with the technique of link smearing. Here one couples the fermions to a smoother gauge link, defined by averaging with adjacent links in a gauge invariant manner. Several closely related implementations are being used. All reduce the coupling of fermions to the short-distance fluctuations in the gauge field, leading to an improvement in the numerical stability and speed of algorithms. One cannot perform this smearing too aggressively, however, since the smearing may distort short distance physics and enhance discretization errors.

As noted above, each fermion formulation has its own advantages and disadvantages. For instance, domain-wall and overlap fermions are theoretically preferred as they have chiral symmetry without doublers, but their computational cost is greater than for other choices. If the physics application of interest and the target precision do not require near-exact chiral symmetry, there is no strong motivation to use these expensive formulations. On the other hand, there is a class of applications (including the calculation of the $\Delta I = 1/2$ amplitude for $K \to \pi\pi$ decays [35–37] and the S-parameter [38]) where chiral symmetry plays an essential role and for which the use of Ginsparg-Wilson fermions is strongly favored.

17.1.3 *Heavy quarks on the lattice*

The fermion formulations described in the previous subsection can be used straightforwardly only for quarks whose masses are small compared to the lattice cutoff, $m_q \lesssim 1/a$. This is because there are discretization errors proportional to powers of am_q, and if $am_q \gtrsim 1$ these errors can become large and uncontrolled. Present LQCD simulations typically have cutoffs in the range of $1/a$ = 2–5 GeV (corresponding to $a \approx$ 0.1–0.04 fm). Thus, while for the up, down and strange quarks one has $am_q \ll 1$, for bottom quarks (with $m_b \approx$ 4.5 GeV) one must use alternative approaches on all but the finest lattices. Charm quarks ($m_c \approx$ 1.5 GeV) are an intermediate case, allowing simulations with either direct or alternative approaches, although increasingly the direct approach is being used.

For the charm quark, the straightforward approach is to simultaneously reduce the lattice spacing and to improve the fermion action so as to reduce the size of errors proportional to powers of am_c. This approach has been followed successfully using the HISQ, twisted-mass and domain-wall actions [24, 25, 27, 39–41]. It is important to note, however, that reducing a increases the computational cost because an increased number of lattice points are needed for the same physical volume. One cannot reduce the spatial size below 2–3 fm without introducing significant finite volume errors. Present lattices have typical sizes of $\sim 64^3 \times 128$ (with the long direction being Euclidean time), and thus allow a lattice cutoff up to $1/a \sim$ 4–6 GeV.

This approach can, to some extent, be extended to the bottom quark, by the use of simulations with small lattice spacings [26,42]. This has been pursued with the HISQ action [43], using lattices of size up to $144^3 \times 288$ and lattice spacings down to $a \approx$ 0.03 fm ($1/a \approx$ 6.6 GeV). Extrapolation in m_b is still needed [44], however, and this makes use of the mass dependence predicted by Heavy Quark Effective Theory (HQET) when heavy-light hadrons are being studied. Small lattice spacings are also helpful for the simulations of quarkonium for which a different heavy-quark mass scaling

is expected. See Ref. [45] for a recent study.

Alternative approaches for discretizing heavy quarks are motivated by effective field theories. For a bottom quark in heavy-light hadrons, one can use HQET to expand about the infinite quark-mass limit. In this limit, the bottom quark is a static color source, and one can straightforwardly write the corresponding lattice action [46]. Corrections, proportional to powers of $1/m_b$, can be introduced as operator insertions, with coefficients that can be determined non-perturbatively using existing techniques [47]. This method allows the continuum limit to be taken systematically including the $1/m_b$ corrections.

Another way of introducing the $1/m_b$ corrections is to include the relevant terms in the effective action. This leads to a non-relativistic QCD (NRQCD) action, in which the heavy quark is described by a two-component spinor [48]. This approach has the advantage over HQET that it can also be used for heavy-heavy systems, such as the Υ states. Moreover, the bottom quark can be treated without any extrapolation in m_b. A disadvantage is that some of the parameters in this effective theory are determined perturbatively (at tree-level or at one-loop [49]), which limits the precision of the final results. Although discretization effects can be controlled with good numerical precision for a range of lattice spacings, these artifacts cannot be extrapolated away by taking the lattice spacing to zero. This is because NRQCD is a non-relativistic effective field theory and so ceases to work when the cutoff π/a becomes much larger than the heavy-quark mass. In practice these effects are accounted for in the error budget.

This problem can be avoided if one uses HQET power counting to analyze and reduce discretization effects for heavy quarks while using conventional fermion actions [50]. For instance, one can tune the parameters of an improved Wilson quark action so that the leading HQET corrections to the static quark limit are correctly accounted for. As the lattice spacing becomes finer, the action smoothly goes over to that of a light Wilson quark action, where the continuum limit can be taken as usual. In principle, one can improve the action in the heavy quark regime up to arbitrarily high orders using HQET, but so far large-scale simulations have typically used clover improved Wilson quarks, where tuning the parameters of the action corresponds to including all corrections through next-to-leading order in HQET. Three different methods for tuning the parameters of the clover action are being used: the Fermilab [50], Tsukuba [51] and Columbia [52] approaches. An advantage of this HQET approach is that the c and b quarks can be treated on the same footing. Parameter tuning has been done perturbatively, as in NRQCD, or using non-perturbative tuning of some of the parameters [53, 54]. One can improve the effective theory including the terms beyond the next-to-leading order. The Oktay-Kronfeld action that includes dimension-six and -seven operators has been constructed [55] and used in large-scale numerical calculations [56].

Another approach is the "ratio method" introduced in Ref. [57]. Here one uses quarks with masses lying at, or slightly above, the charm mass m_c, which can be simulated with a relativistic action, and extrapolates to m_b incorporating the behavior predicted by HQET. The particular implementation relies on the use of ratios. As an example, consider the B meson decay constant f_B. According to HQET, this scales as $1/\sqrt{m_B}$ for $m_B \gg \Lambda_{\rm QCD}$, up to a logarithmic dependence that is calculable in perturbative QCD (but will be suppressed in the following). Here m_B is the B meson mass, which differs from m_b by $\sim \Lambda_{\rm QCD}$. One considers the ratio $y(\lambda, m_{b'}) \equiv f_{B''}\sqrt{m_{B''}}/f_{B'}\sqrt{m_{B'}}$ for fictitious B mesons containing b quarks with unphysical masses $m_{b'}$ and $m_{b''} = \lambda m_{b'}$. HQET implies that $y(\lambda, m_{b'})$ approaches unity for large $m_{b'}$ and any fixed $\lambda > 1$. The ratios are evaluated on the lattice for the sequence of masses $m_{b'} = m_c$, λm_c, $\lambda^2 m_c$, all well below the physical m_b, and for each the continuum limit is taken. The form of the ratio for larger values of $m_{b'}$ is obtained by fitting, incorporating the constraints implied by HQET. The result for $f_B\sqrt{m_B}$ is then obtained as a product of y's with $f_D\sqrt{m_D}$ [58].

17.1.4 *QED on the lattice*

Quarks in nature are electrically charged, and the resultant coupling to photons leads to shifts in the properties of hadrons that are generically of $\mathcal{O}(\alpha_{\rm EM})$. Thus, for example, the proton mass is increased by ~ 1 MeV relative to that of the neutron due to its overall charge although this effect is more than compensated for by the ~ 2.5 MeV relative decrease due to the up quark being lighter than the down quark [59]. This example shows that once pure QCD, isospin-symmetric lattice calculations reach percent-level accuracy, further improvement requires the inclusion of effects due to both electromagnetism and the up-down mass difference. This level of accuracy has in fact been obtained for various quantities, e.g., light hadron masses and decay constants (see Ref. [60]), and simulations including isospin-breaking and QED effects are becoming more common.

One approach for including QED is to treat electromagnetic gauge fields in a similar fashion to those of QCD. This extension is straightforward, although some new subtleties arise. The essential change is that the quark must now propagate through a background field containing both gluons and photons. The gauge field U_μ that appears in the covariant derivative of Eq. (17.3) is extended from an SU(3) matrix to one living in U(3): $U_\mu \to U_\mu e^{iaqeA_\mu^{\rm EM}}$. Here $A_\mu^{\rm EM}$ is the photon field, e the electromagnetic coupling, and q the charge of the quark, e.g., $q = 2/3$ for up and $-1/3$ for down and strange quarks. The lattice action for the photon that is typically used is a discretized version of the continuum action Eq. (17.2), rather than the form used for the gluons, Eq. (17.1). This "non-compact" action has the advantage that it is quadratic in $A_\mu^{\rm EM}$, which simplifies the QED part of the generation of configurations.

One subtlety that arises is that Gauss' law forbids a charged particle in a box with periodic boundary conditions. This can be overcome by including a uniform background charge, which can be shown to be equivalent to removing the zero-momentum mode from the photon field, an approach denoted QED$_L$ [61]. However, this modification leads to enhanced finite-volume dependence for physical quantities, scaling as $1/L^n$ with $n = 1, 2, \cdots$. This should be compared to the $\exp(-m_\pi L)$ dependence expected for many quantities (as discussed in Sec. 17.1.6.2 below). Methods to remove the leading few powers of $1/L$ have been developed [62, 63], and there is a promising alternative approach in which QED effects are calculated analytically in infinite volume [64]. Finally we note that there is an alternative approach using so-called C^* boundary conditions that avoids the Gauss' law issue altogether, although the numerical application is still at an early stage [65, 66].

Substantial progress on including QED and isospin-breaking effects has been made over the last few years. The direct approach of using different up and down-quark masses and simulating QED has been successfully carried out for a range of quark masses approaching the physical values [59, 67–69]. Alternative approaches have also been used: reweighting the QCD fields *a posteriori* [70], using a massive photon [71], and keeping only the linear term in an expansion in $\alpha_{\rm EM}$ about the QCD only case [72, 73], with the latter approach by now the most popular. Most calculations to date have included QED effects for the valence quarks but not the sea quarks (the "electro-quenched approximation"). [41, 74–77].

The QED corrections to processes including leptons, such as the leptonic and semileptonic decays of hadrons, involve additional diagrams in which a photon propagator bridges between a hadron and a lepton. Such diagrams induce infrared divergences that cancel against soft photon radiation (Bloch-Nordsieck theorem [78]). Methods have been developed to implement this cancellation in lattice calculations, treating the soft photon analytically [62], and results have been reported for leptonic pion and kaon decays [79–81]. An application to semi-leptonic decays has been developed [64, 82].

17.1.5 *Basic inputs for lattice calculations*

Since LQCD is nothing but a regularization of QCD, the renormalizability of QCD implies that the number of input parameters in LQCD is the same as for continuum QCD—the strong gauge coupling $\alpha_s = g^2/(4\pi)$, the quark masses for each flavor, and the CP violating phase $\theta_{\rm QCD}$. The $\theta_{\rm QCD}$ parameter is usually assumed to be zero, while the other parameters must be determined using experimental inputs.

17.1.5.1 *Lattice spacing*

In QCD, the gauge coupling is a function of scale. With lattice regularization, this scale is the inverse lattice spacing $1/a$, and choosing the bare gauge coupling is equivalent to fixing the lattice spacing.

In principle, a can be determined using any dimensionful quantity measured accurately by experiments. For example, using the mass of hadron H one has $a = (am_H)^{\rm lat}/m_H^{\rm exp}$. One chooses quantities that can be calculated accurately on the lattice, and that are only weakly dependent on the quark masses. The latter property minimizes errors from extrapolating or interpolating to the physical light quark masses or from mistuning of other quark masses.

Commonly used choices are the spin-averaged 1S-1P or 1S-2S splittings in the Υ system, the masses of the Ξ and Ω^- baryons, and the pion decay constant f_π. Ultimately, all choices must give consistent results for physical quantities in the continuum limit, and that this is the case provides a highly non-trivial check of both the calculational method and of QCD.

Many recent lattice calculations use intermediate length scales in place of a direct determination of the lattice spacing. These length scales, which we denote $\mathcal{R}$, have the advantage that they can be precisely, and relatively cheaply, computed numerically. Examples are r_0, derived from the heavy quark potential [83], and t_0 and w_0, determined from the gradient flow of the gauge field [84]. These scales are used in the following manner, explained here in the context of calculating a quantity Q with mass dimension d (e.g. a decay constant for which $d = 1$). In the first step, one calculates the dimensionless quantities a^dQ and $\mathcal{R}/a$ in a given lattice calculation, and forms the product $(a^dQ) \times (\mathcal{R}/a)^d = Q\mathcal{R}^d$. In a second step, one uses results available from previous dedicated lattice calculations that have determined $\mathcal{R}$ in physical units (i.e. fm) by relating it to a physical quantity as discussed above. Then one obtains $Q = (Q\mathcal{R}^d)/\mathcal{R}^d$. The use of intermediate quantities is reviewed in the latest edition of the Flavor Lattice Averaging Group (FLAG) report [85].

17.1.5.2 *Light quark masses*

In LQCD simulations, the up, down and strange quarks are usually referred to as the light quarks, in the sense that $m_q < \Lambda_{\rm QCD}$. (The standard definition of $\Lambda_{\rm QCD}$ is given in the "Quantum Chromodynamics" review; in this review we are using it only to indicate the approximate non-perturbative scale of QCD.) This condition is stronger than that used above to distinguish quarks with small discretization errors, $m_q < 1/a$. Loop effects from light quarks must be included in the simulations to accurately represent QCD. At present, most simulations are done in the isospin symmetric limit $m_u = m_d \equiv m_\ell < m_s$, with charm-quark loops either excluded (referred to as "$N_f = 2 + 1$" simulations) or included (denoted "$N_f = 2 + 1 + 1$" simulations). As noted above, precision is now reaching the point where isospin breaking effects must be included. To do so without approximation requires simulating with non-degenerate up and down quarks (leading to $N_f = 1 + 1 + 1$ or $1 + 1 + 1 + 1$ simulations) as well as including electromagnetism (as described above).

We now describe the tuning of m_ℓ, m_s and m_c to their physical values. (For brevity, we ignore isospin violation in the following discussion.) The most commonly used quantities for these tunings are, respectively, m_π, m_K and m_{η_c} or m_{D_s}. If the scale is being set by m_Ω, then one adjusts the lattice quark masses until the ratios m_π/m_Ω, m_K/m_Ω and m_{η_c}/m_Ω take their physical values. In

the past, most calculations needed to extrapolate to the physical value of m_ℓ (typically using forms based on chiral perturbation theory [ChPT]), while simulating directly at or near to the physical values of m_s and m_c. Present calculations are increasingly done with physical or near physical values of m_ℓ, requiring at most only a short extrapolation or interpolation.

17.1.5.3 *Heavy quark masses*

The b quark is usually treated only as a valence quark, with no loop effects included. The errors introduced by this approximation can be estimated to be $\sim \alpha_s(m_b)\Lambda^2_{\rm QCD}/m_b^2$ and are likely to be very small. In the past, the same approximation has been made for the c quark, leading to errors $\sim \alpha_s(m_c)\Lambda^2_{\rm QCD}/m_c^2$. (See Ref. [86] for a quantitative estimate of the effects of including the charm quark on some low energy physical quantities, and Ref. [87] for similar estimates for B-meson matrix elements.) For high precision, however, dynamical charm quarks are necessary, and many of the most recent simulations now include them.

The b quark mass can be tuned by setting heavy-heavy (Υ) or heavy-light (B or B_s) meson masses to their experimental values. Consistency between these two determinations provides an important check that the determination of parameters in the heavy quark lattice formulations is being done correctly (see, e.g., Ref. [26, 88, 89]). For instance, the b quark masses obtained from heavy-light [44] and heavy-heavy [77] mesons are in excellent agreement within the precision of 0.5%.

17.1.6 *Sources of systematic error*

Lattice results have statistical and systematic errors that must be quantified for any calculation in order for the result to be a useful input to phenomenology. The statistical error is due to the use of Monte Carlo importance sampling to evaluate the path integral (a method discussed below). There are, in addition, a number of systematic errors that are always present to some degree in lattice calculations, although the size of any given error depends on the particular quantity under consideration and the parameters of the ensembles being used. The most common lattice errors are reviewed below.

Although not strictly a systematic error, it is important to note that the presence of long autocorrelations in the sequence of lattice configurations generated by the Monte Carlo method can lead to underestimates of statistical errors [90]. It is known that the global topological charge of the gauge fields decorrelates very slowly with certain algorithms, especially when the lattice spacing is small [90, 91]. The effect of poorly sampling topological charge is expected to be most significant for the pion mass and related quantities [92–94]. This issue becomes more relevant as the precision of the final results improves. The problem of slow decorrelation of topology can be mitigated using open boundary conditions, for which the global topological charge is not quantized [95].

17.1.6.1 *Continuum limit*

Physical results are obtained in the limit that the lattice spacing a goes to zero. Symanzik effective theory determines the scaling of lattice artefacts with a. Most lattice calculations use improved actions with leading discretization errors of $\mathcal{O}(\alpha_s a\Lambda)$, $\mathcal{O}(a^2\Lambda^2)$, or $\mathcal{O}(\alpha_s a^2\Lambda^2)$, where Λ is a typical momentum scale in the system. Knowledge of the scaling of the leading discretization errors allows controlled extrapolation to $a = 0$ when multiple lattice spacings are available, as in current state-of-the-art calculations. Terms that allow for higher powers of a are usually included in the fit form for the continuum extrapolation, with either loosely constrained or unconstrained coefficients, to be determined by the fit. There is also sub-leading a dependence with pre-factors containing powers of $\log a$. This can, in principle, be understood using the Symanzik effective theory, and first studies of this have been undertaken [96–98].

For many quantities, the typical momentum scale in the system is $\Lambda_{\rm QCD} \approx 300$ MeV. Discretiza-

tion errors are expected to be larger for quantities involving larger scales, for example form factors or decays involving particles with momenta or masses larger than $\Lambda_{\rm QCD}$.

17.1.6.2 *Infinite volume limit*

LQCD calculations are necessarily carried out in finite space-time boxes, leading to departures of physical quantities (masses, decay constants, etc.) from their measured, infinite volume values. These finite-volume shifts are an important systematic that must be estimated and minimized.

Typical lattices are asymmetric, with N_s points in the three spatial directions and N_t in the (Euclidean) temporal direction. The spatial and temporal sizes in physical units are thus $L_s = aN_s$ and $L_t = aN_t$, respectively. (Anisotropic lattice spacings are also sometimes used, as discussed below in Sec. 17.2.2.) Typically, $L_t \geq 2L_s$, a longer temporal direction being used to allow excited-state contributions to correlators to decay. This means that the dominant impact of using finite volume is from the presence of a finite spatial box.

The highest-precision LQCD calculations are of quantities involving no more than a single strongly-interacting particle in initial and final states. For such quantities, once the spatial size exceeds about 2 fm (so that the particle is not "squeezed"), the dominant finite-volume effect comes from virtual pions wrapping around the lattice in the spatial directions. This effect is exponentially suppressed as the volume becomes large, roughly as $\sim \exp(-m_\pi L_s)$, and has been estimated using ChPT [99] or other methods [100]. These estimates suggest that finite volume shifts are sub-percent effects when $m_\pi L_s \gtrsim 4$, and most large-scale simulations use lattices satisfying this condition. (See also Sec. 2.1.1 of the FLAG report [85] for more detailed discussion concerning the conditions required to control finite-volume effects.) This becomes challenging as one approaches the physical pion mass, for which $L_s \gtrsim 5$ fm is required.

Finite-volume errors are usually determined by repeating the simulations on two or more different volumes (with other parameters fixed). If different volumes are not available, the ChPT estimate can be used, often inflated to account for the fact that the ChPT calculation is truncated at some order.

LQCD calculations involving more than a single hadron are becoming increasingly precise. Examples include the calculation of resonance parameters and the $K \to \pi\pi$ amplitudes. Finite-volume effects are much larger in these cases, with power-law terms (e.g., $1/L_s^3$) in addition to exponential dependence. Indeed, as will be discussed in Sec. 17.2.4, one can use the volume dependence to indirectly extract infinite-volume quantities such as scattering lengths. Doing so, however, requires a set of lattice volumes satisfying $m_\pi L_s \gtrsim 4$ and is thus more challenging than for single-particle quantities.

17.1.6.3 *Chiral extrapolation*

Until recently, an important source of systematic error in LQCD calculations was the need to extrapolate in m_u and m_d (or, equivalently, in m_π). This extrapolation was usually done using functional forms based on ChPT, or with analytic functions, with the difference between different fits used as an estimate of the systematic error, which was often substantial. Increasingly, however, calculations work directly at, or very close to, the physical quark masses. This either removes entirely, or greatly reduces, the uncertainties in the extrapolation, such that this error is subdominant.

17.1.6.4 *Operator matching*

Many of the quantities that LQCD can precisely calculate involve hadronic matrix elements of operators from the electroweak Hamiltonian. Examples include the pion and kaon decay constants, semileptonic form factors and the kaon mixing parameter B_K (the latter defined in Eq. (17.13)). The operators in the lattice matrix elements are defined in the lattice regularization scheme. To be

used in tests of the Standard Model, however, they must be matched to the continuum regularization scheme in which the corresponding Wilson coefficients have been calculated. The only case in which such matching is not needed is if the operator is a conserved or partially conserved current. Similar matching is also needed for the conversion of lattice bare quark masses to those in the continuum $\overline{\rm MS}$ scheme.

Several methods are used to calculate the matching factors: perturbation theory (usually to one- or two-loop order), non-perturbative renormalization (NPR) using Landau-gauge quark and gluon external states [101], NPR based on the Schrödinger functional [102], NPR using short-distance hadron correlators [103], and NPR using heavy-heavy correlators [27, 104]. The NPR methods replace truncation errors from perturbation theory (which can only be estimated approximately) by statistical and systematic errors that can be determined reliably and systematically reduced.

An issue that arises in some of such calculations (e.g., for quark masses and B_K) is that, using NPR with Landau-gauge quark and gluon external states, one ends up with operators regularized in a MOM-like scheme (or a Schrödinger-functional scheme), rather than the $\overline{\rm MS}$ scheme mostly used for calculating the Wilson coefficients. To make contact with this scheme requires a purely continuum perturbative matching calculation supplemented by the operator product expansion (OPE). (The importance of power corrections is emphasized in [105].) The resultant truncation error of perturbative expansion and OPE can be minimized by pushing up the momentum scale at which the matching is done using step-scaling techniques as part of the NPR calculation [106].

It should also be noted that this final step in the conversion to the $\overline{\rm MS}$ scheme could be avoided if continuum calculations used a MOM-like scheme or if one imposes a renormalization condition for quantities that are calculable both in the $\overline{\rm MS}$ scheme and in LQCD, such as the hadron correlators at short distances (see, e.g., Ref. [107]).

17.2 Methods and status

Once the lattice action is chosen, it is straightforward to define the quantum theory using the path integral formulation. The Euclidean-space partition function is

$$Z = \int [dU] \prod_f [dq_f][d\bar{q}_f] e^{-S_g[U] - \sum_f \bar{q}_f (D[U]+m_f) q_f} \,, \tag{17.4}$$

where link variables are integrated over the SU(3) manifold, q_f and $\bar{q}_f$ are Grassmann (anti-commuting) quark and antiquark fields of flavor f, and $D[U]$ is the chosen lattice Dirac operator with m_f the quark mass in lattice units. Integrating out the quark and antiquark fields, one arrives at a form suitable for simulation:

$$Z = \int [dU] e^{-S_g[U]} \prod_f \det(D[U] + m_f) \,. \tag{17.5}$$

The building blocks for calculations are expectation values of multi-local gauge-invariant operators, also known as "correlation functions",

$$\langle \mathcal{O}(U,q,\bar{q}) \rangle = (1/Z) \int [dU] \prod_f [dq_f][d\bar{q}_f] \mathcal{O}(U,q,\bar{q}) e^{-S_g[U] - \sum_f \bar{q}_f (D[U]+m_f) q_f} \,. \tag{17.6}$$

If the operators depend on the (anti-)quark fields q_f and $\bar{q}_f$, then integrating these fields out leads not only to the fermion determinant but also, through Wick's theorem, to a series of quark "propagators", $(D[U] + m_f)^{-1}$, connecting the positions of the fields.

This set-up allows one to choose, by hand, the masses of the quarks in the determinant (the sea quarks) differently from those in the propagators (valence quarks). This is called "partial quenching", and is used by some calculations as a way of obtaining more data points from which to extrapolate both sea and valence quarks to their physical values.

17.2.1 *Monte-Carlo method*

Since the number of integration variables U is huge ($N_s^3 \times N_t \times 4 \times 8$), direct numerical integration is impractical and one has to use Monte-Carlo techniques. In this method, one generates a Markov chain of gauge configurations (a "configuration" being the set of U's on all links) distributed according to the probability measure $[dU]e^{-S_g[U]} \prod_f \det(D[U] + m_f)$. Once the configurations are generated, expectation values $\langle O(U, q, \bar{q})\rangle$ are calculated by averaging over those configurations. In this way the configurations can be used for many different calculations, and there are several large collections of ensembles of configurations (with a range of values of a, lattice sizes and quark masses) that are publicly available through the International Lattice Data Grid (ILDG) [108].

The most challenging part of the generation of gauge configurations is the need to include the fermion determinant. Direct evaluation of the determinant is not feasible, as it requires $\mathcal{O}((N_s^3 \times N_t)^3)$ computations. Instead, one rewrites it in terms of "pseudo-fermion" fields ϕ (auxiliary fermion fields with bosonic statistics). For example, for two degenerate quarks one has

$$\det(D[U] + m_f)^2 = \int [d\phi] e^{-\phi^\dagger ((D[U]+m_f)(D[U]+m_f)^\dagger)^{-1}\phi} . \tag{17.7}$$

By treating the pseudo-fermions as additional integration variables in the path integral, one obtains a totally bosonic representation. The price one pays is that the pseudo-fermion effective action is highly non-local since it includes the inverse Dirac operator $(D[U] + m_f)^{-1}$. Thus, the large sparse matrix $(D[U] + m)$ has to be inverted every time one needs an evaluation of the effective action.

Present simulations generate gauge configurations using the Hybrid Monte Carlo (HMC) algorithm [109], or variants thereof. This algorithm combines molecular dynamics (MD) evolution [110–112] in a fictitious time (which is also discretized) with a Metropolis "accept-reject" step [113]. It makes a global update of the configuration, and is made exact by the Metropolis step. In its original form it can be used only for two degenerate flavors, but extensions (particularly the rational HMC [114]) are available for single flavors. Considerable speed-up of the algorithms has been achieved over the last two decades using a variety of techniques.

All these algorithms spend the bulk of their computational time on the repeated inversion of $(D[U] + m)$ acting on a source (which is required at every step of the MD evolution). Inversions are done using a variety of iterative algorithms, e.g., the conjugate gradient algorithm. In this class of algorithms, computational cost is determined by the condition number of the matrix, which is the ratio of maximum and minimum eigenvalues. For $(D[U] + m)$ the smallest eigenvalue is $\approx m$, and the cost is inversely proportional to the quark mass. This is a major reason why simulations at the physical light quark masses are challenging.

Algorithmic improvements have significantly reduced this problem. The main idea is to separate different length scales [115, 116]. Since the low eigenvalues of $(D[U] + m)$ are associated with long wavelength quark modes, one may project the problem onto that of a coarse-grained lattice by averaging the field within a block of sublattices and carrying out the inversion on this coarse lattice. The result is then fed back to the original lattice as an efficient *preconditioner* for the iterative solver, and the whole procedure may be nested multiple times. Variants of such methods have been implemented, specifically domain-decomposition [117, 118], deflation [119–122] and multigrid [123, 124]. They are increasingly used in large-scale lattice simulations.

A practical concern is the inevitable presence of correlations between configurations in the Markov chain. These are characterized by an auto-correlation length in the fictitious MD time. One aims to use configurations separated in MD time by greater than this auto-correlation length. Then, as the number of decorrelated configurations, N, is increased, the statistical error decreases as $1/\sqrt{N}$. In practice, it is difficult to measure this length accurately, see, for example, [125]. This,

as well as the possibility of insufficient equilibration leads to some uncertainty in the resulting statistical errors.

The computational cost of gauge generation grows with the lattice volume, $V_{\rm lat} = N_s^3 N_t$, as $V_{\rm lat}^{1+\delta}$. Here $\delta = 1/4$ for the HMC algorithm [126] and can be reduced slightly using modern variants. Such growth with $V_{\rm lat}$ provides a (time-dependent) limit on the largest lattice volumes that can be simulated. At present, the largest lattices being used have $N_s = 144$ and $N_t = 288$ or $N_s = N_T = 160$. Typically, one aims to create an ensemble of $\sim 10^3$ statistically independent configurations at each choice of parameters (a, m_q and $V_{\rm lat}$). For most physical quantities of interest, this is sufficient to make the resulting statistical errors smaller than or comparable to the systematic errors. Recently, the master-field approach is being investigated [13, 127, 128]. It aims to create a large-volume ensemble and repeat the calculation of physical quantities in different small patches of the entire lattice. Translational invariance guarantees that the correct average is obtained with fewer configurations than in the traditional approach, with the advantage of reduced finite-volume effects [129].

In the past, the cost of generating gauge configurations was larger than that of performing "measurements" on those configurations. However, as the number of quantities being calculated and their complexity has increased, the balance has shifted to the point that the total cost of measurements exceeds that of generation. Sharing the configurations, e.g. through the ILDG, has become more common, and a number of groups are utilizing them to compute a wide variety of quantities, as partly covered by the following sections.

17.2.2 *Two-point functions*

One can extract properties of stable hadrons from two-point correlation functions, $\langle O_X(x) O_Y^\dagger(0)\rangle$. Here $O_{X,Y}(x)$ are operators that have non-zero overlaps with the hadronic state of interest $|H\rangle$, *i.e.* $\langle 0|O_{X,Y}(x)|H\rangle \neq 0$. On the lattice, the two-point correlation function can be constructed, using Wick's theorem, from the quark propagators $(D[U] + m_f)^{-1}_{x0}$ from the insertion point of the source operator $O_Y(0)$ to the sink operator $O_X(x)$ (see Fig. 17.2). An average over gauge configurations yields the estimate of $\langle O_X(x) O_Y^\dagger(0)\rangle$ for all x on the lattice.

One usually Fourier transforms in the spatial directions and considers correlators as a function of Euclidean time:

$$C_{XY}(t;\boldsymbol{p}) = \sum_{\boldsymbol{x}} \langle O_X(t,\boldsymbol{x}) O_Y^\dagger(0)\rangle e^{-i\boldsymbol{p}\cdot\boldsymbol{x}}. \tag{17.8}$$

(Here and throughout this section all quantities are expressed in dimensionless lattice units, so that, for example, $\boldsymbol{p} = a\boldsymbol{p}_{\rm phys}$.) By inserting a complete set of states having spatial momentum $\boldsymbol{p}$, the two-point function can be written as

$$C_{XY}(t;\boldsymbol{p}) = \sum_{i=0}^{\infty} \frac{1}{2E_i(\boldsymbol{p})} \langle 0|O_X(0)|H_i(\boldsymbol{p})\rangle \langle H_i(\boldsymbol{p})|O_Y^\dagger(0)|0\rangle e^{-E_i(\boldsymbol{p})t}, \tag{17.9}$$

where the energy of the i-th state $E_i(\boldsymbol{p})$ appears in the eigenvalue of the Euclidean time evolution operator e^{-Ht}, $e^{-E_i(\boldsymbol{p})t}$. The factor of $1/[2E_i(\boldsymbol{p})]$ is due to the relativistic normalization used for the states. For large enough t, the dominant contribution is that of the lowest energy state $|H_0(\boldsymbol{p})\rangle$:

$$C_{XY}(t;\boldsymbol{p}) \overset{t\to\infty}{\longrightarrow} \frac{1}{2E_0(\boldsymbol{p})} \langle 0|O_X(0)|H_0(\boldsymbol{p})\rangle \langle H_0(\boldsymbol{p})|O_Y^\dagger(0)|0\rangle e^{-E_0(\boldsymbol{p})t}\,. \tag{17.10}$$

One can thus obtain the energy $E_0(\boldsymbol{p})$, which equals the hadron mass m_H when $\boldsymbol{p} = 0$, and the product of matrix elements $\langle 0|O_X(0)|H_i(\boldsymbol{p})\rangle \langle H_i(\boldsymbol{p})|O_Y^\dagger(0)|0\rangle$.

This method can be used to determine the masses of all the stable (in QCD) mesons and baryons by making appropriate choices of operators. For example, if one uses the axial current,

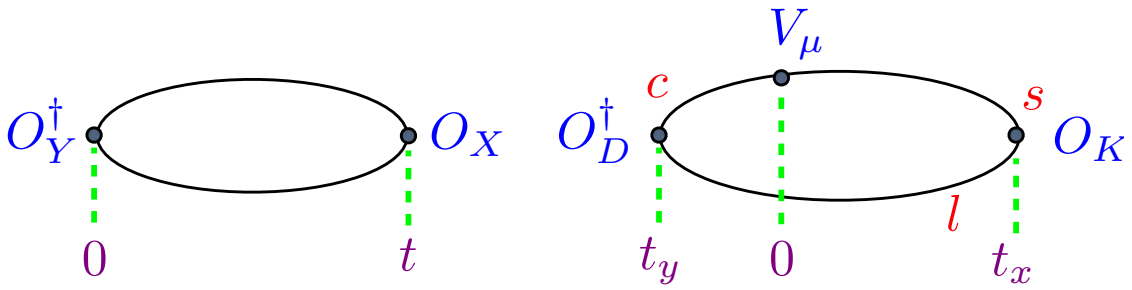

Figure 17.2: Schematic diagrams of a two-point correlation function (left) and three-point correlation function (right). Solid lines represent quark or antiquark propagators obtained by solving the Dirac equation with a source. For the two-point correlation function the quark and antiquark propagators from the source point $t = 0$ are multiplied together at each t value with appropriate γ matrices in between, corresponding to the operators $O_Y^\dagger$ and O_X. Traces are performed over spin and color and, usually, a sum over spatial positions at the sink t (see Eq. (17.8)). The three-point correlation function corresponds to that of Eq. (17.11), with the flavors of the quark propagators marked ($l = u/d$). Typically this calculation would be done by using the l propagator from t_x at timeslice t_y, after multiplication by appropriate γ matrices for O_D, as a source for the c propagator. The c and s propagators are then tied together at $t = 0$ after inserting γ_μ.

$O_X = O_Y = A_\mu = \bar{d}\gamma_\mu\gamma_5 u$, then one can determine m_{π^+} from the rate of exponential fall-off, and in addition the decay constant f_π from the coefficient of the exponential since $\langle 0|A_\mu|\pi\rangle = f_\pi p_\mu$.

Because of its dominance at large times, the lowest energy ground-state is the one most accurately characterized from the lattice analysis of the correlator $C_{XY}(t;\boldsymbol{p})$. How accurately the ground-state parameters can be determined depends on the quantum numbers and quark content of H_0, however. This is because the statistical variance in $C_{XY} \sim \langle O_X O_Y^\dagger\rangle$ is controlled by $\langle (O_X O_Y^\dagger)^2\rangle$, itself a correlation function containing a set of states in a similar way to Eq. (17.9) [130,131]. In the best-case scenario the ground-state of $\langle (O_X O_Y^\dagger)^2\rangle$ is two H_0 mesons with energy close to $2E_0$. Then the signal/noise ratio in C_{XY} is approximately independent of t and the accurate long-time tail of C_{XY} is useful in obtaining high statistical precision on E_0 and the ground-state amplitude. This is the situation for flavour-diagonal pseudoscalar mesons. For unequal valence quark masses, the signal/noise ratio falls exponentially in time t with an exponent given by $m_{Q\bar{q}} - (m_{Q\bar{Q}} + m_{q\bar{q}})/2$, where $m_{Q\bar{q}}$ denotes the pseudoscalar meson mass composed of flavor Q and q and so on. This has a small impact for the kaon, but it is a bigger problem for the B mesons, increasing the statistical uncertainty in the ground-state parameters. The signal/noise issue is also significant for light vector mesons and baryons; for ρ meson correlators, the signal/noise falls exponentially with exponent $m_\rho - m_\pi$ and for the nucleon, $m_N - 3m_\pi/2$. This limits the range of useful t values in the correlator fits. The same issue is responsible for growing statistical noise in $C_{XY}(t;\boldsymbol{p})$ as $|\boldsymbol{p}|$ is increased. Mitigation strategies include using efficient methods for calculating quark propagators, such as all-mode-averaging [132], which allows one to increase the number of samples, as well as using multi-level Monte-Carlo methods that can reduce the growth of the uncertainty with distance [133].

The expression given in (17.9) for the correlator $C_{XY}(t;\boldsymbol{p})$ shows how, in principle, one can determine the energies of the excited hadron states having the same quantum numbers as the operators $O_{X,Y}$, by fitting the correlation function to a sum of exponentials, including both ground-state and excited-state contributions. It is important to do this in order to obtain accurate results

for the ground-state parameters. To reliably identify excited-state parameters in practice, one often needs to use a large basis of operators with a variety of overlaps, $\langle 0|O_X|H_i\rangle$ with the different states, and to adopt a variational approach, such as that of [134]. The use of anisotropic lattices in which a_t, the lattice spacing in the time direction, is smaller than its spatial counterpart, a_s, allows for more temporal samples of the correlation function at small times where there is a signal for excited states. Using these and and other technical improvements, extensive excited-state spectra have been obtained [135–140].

A complication arises for states with high spins ($j \geq 4$ for bosons) because the spatial rotation group on the lattice is a discrete subgroup of the continuum group SO(3). This implies that lattice operators, even when chosen to lie in irreducible representations of the lattice rotation group, have overlap with states that have a number of values of j in the continuum limit [141]. For example $j = 0$ operators can also create mesons with $j = 4$. Methods to overcome this problem in practice are available [135, 142] and have been used successfully.

The two-point function (17.8) contains, in principle, information on all possible states having the quantum numbers of the operator O. Thus, if O is chosen to be a vector current, it can be used to estimate the hadronic vacuum polarization function contribution to the muon anomalous magnetic moment, as discussed in Sec. 17.3.7.

17.2.3 *Three-point functions*

Hadronic matrix elements needed to calculate semileptonic form factors and neutral meson mixing amplitudes can be computed from three-point correlation functions. We discuss here, as a representative example, the $D \to K$ amplitude (see Fig. 17.2). As in the case of two-point correlation functions one constructs operators O_D and O_K having overlap, respectively, with the D and K mesons. We are interested in calculating the matrix element $\langle K|V_\mu|D\rangle$, with $V_\mu = \bar{c}\gamma_\mu s$ the flavor-changing vector current.

To obtain this, we use the three-point correlator constructed from three quark propagators

$$C_{KV_\mu D}(t_x, t_y; \boldsymbol{p}) = \sum_{\boldsymbol{x},\boldsymbol{y}} \langle O_K(t_x, \boldsymbol{x}) V_\mu(0) O_D^\dagger(t_y, \boldsymbol{y})\rangle e^{-i\boldsymbol{p}\cdot\boldsymbol{x}}\,, \tag{17.11}$$

and focus on the limit $t_x \to \infty$, $t_y \to -\infty$. In this example we set the D-meson at rest while the kaon carries three-momentum $\boldsymbol{p}$. Momentum conservation then implies that the weak operator V_μ inserts three-momentum $-\boldsymbol{p}$. Inserting a complete set of states between each pair of operators, we find

$$\begin{aligned} C_{KV_\mu D}(t_x, t_y; \boldsymbol{p}) = \sum_{i,j} \frac{1}{2m_{D_i} 2E_{K_j}(\boldsymbol{p})} e^{-m_{D_i} t_x - E_{K_j}(\boldsymbol{p})|t_y|} \\ \times \langle 0|O_K(0)|K_j(\boldsymbol{p})\rangle \langle K_j(\boldsymbol{p})|V_\mu(0)|D_i(\boldsymbol{0})\rangle \langle D_i(\boldsymbol{0})|O_D^\dagger(0)|0\rangle. \end{aligned} \tag{17.12}$$

The matrix element $\langle K_i(\boldsymbol{p})|V_\mu(0)|D_j(\boldsymbol{0})\rangle$ can then be extracted, since all other quantities in this expression can be obtained from two-point correlation functions. Typically, one is interested in the weak matrix elements of ground states, such as the lightest pseudo-scalar mesons. In the limit of large separation between the three operators in Euclidean time, the three-point correlation function yields the weak matrix element of the transition between ground states. Reliable determination of the ground-state matrix element requires the calculation of $C_{KV_\mu D}$ for multiple large values of $t_x - t_y$ so that simultaneous multi-exponential fits to three-point and two-point correlation functions can be done. This is harder for cases such as baryon matrix elements with a significant signal/noise problem (see Sec. 17.2.2). Complications may also arise in cases where a significant contribution is expected from states with an extra pion. An example relevant to $B \to \pi\ell\nu$ decay is discussed in Ref. [143].

From (17.12) the matrix element $\langle K_i(\boldsymbol{p})|V_\mu(0)|D_j(\boldsymbol{0})\rangle$ is obtained at several discretized values of momentum $\boldsymbol{p}$, given by a multiple of $2\pi/L$ in each spatial direction. Each momentum corresponds to a certain value of the momentum transfer $q^2 = (m_D - E_K(\boldsymbol{p}))^2 - \boldsymbol{p}^2$. The restriction on the available momentum can be relaxed by introducing twisted boundary conditions [144–146], which are a generalization of (anti-)periodic boundary conditions in the spatial directions that allows a general $U(1)$ phase upon translation by distance L. The choice of phase leads to a quark momentum that does not have to be a multiple of $2\pi/L$. The method has been applied in a number of lattice calculations.

To interpolate in q^2, the so-called z parametrization [147–150] is often employed. It takes account of the analytic structure of the form factor in the complex q^2 plane, and a polynomial expansion in z is justified.

17.2.4 *Scattering amplitudes and resonances*

The methods described thus far yield matrix elements involving single, stable particles (where by stable we mean here absolutely stable to strong interaction decays). Most of the particles listed in the Review of Particle Properties are, however, unstable—they are resonances decaying into final states consisting of multiple strongly interacting particles. LQCD simulations cannot directly calculate resonance properties, but methods have been developed to do so indirectly for resonances coupled to two- and three-particle final states in the elastic regime, starting from the seminal work of Lüscher [151].

The difficulty faced by LQCD calculations is that, to obtain resonance properties, one must calculate multi-particle scattering amplitudes in momentum space and put the external particles on their mass-shells. This requires analytically continuing from Euclidean to Minkowski momenta. Although it is straightforward in LQCD to generalize the methods described above to calculate four- and higher-point correlation functions, one necessarily obtains them at a discrete and finite set of Euclidean momenta. Analytic continuation to $p_E^2 = -m^2$ is then an ill-posed and numerically challenging problem. The same problem arises for single-particle states, but can be largely overcome by picking out the exponential fall-off of the Euclidean correlator, as described above. With a multi-particle state there is no corresponding trick, except for two particles at threshold [152], although recent ideas using smeared correlators and advanced spectral-reconstruction methods have made significant progress [153–156].

What LQCD can calculate are the energies of the eigenstates of the QCD Hamiltonian in a finite box. The energies of states containing stable particles, e.g., two or three pions, clearly depend on the interactions between the particles. It is possible to invert this dependence and, with plausible assumptions, determine the scattering amplitudes in a limited kinematical range. This is most straightforward in the case of two particles in the elastic regime with a single dominant partial wave, in which case one can obtain the scattering phase-shifts at a discrete set of momenta from a calculation of the two-particle energy levels for a variety of spatial volumes [151]. Determinations of two-meson and meson-nucleon interactions using generalizations of this methodology to multiple channels [157], and particles with spin [158], are now standard, albeit largely with heavier-than-physical quark masses. There is also an alternative approach using a lattice calculation of the Bethe-Salpeter amplitude to determine two-particle interaction potentials [159]. Channels studied include $\pi\pi$, $\bar{K}K$, $K\pi$, $\pi\omega$, $\pi\phi$, KD, DD^*, D^*D^*, $B\pi$, $N\pi$, $\Sigma\pi$, and NK. For results using physical quark masses see [160, 161]; recent comprehensive reviews are [162]. Extensions to two-nucleon interactions are being actively studied [163]; recent reviews are [164]. The formalism has been generalized to three particles (both identical and non-degenerate, and including spin and multiple channels) [165], and has been applied in lattice calculations of $3\pi^+$, $2\pi^+ + K^+$, $\pi^+ + 2K^+$, and $3K^*$ systems [161,166], to the $I = 1$ and 0 three-pion channels [167], and to the $DD\pi$ system [168].

For recent reviews, see [169].

It is also possible to extend the methodology to calculate electroweak decay amplitudes to two particles below the inelastic threshold, e.g., $A(K \to \pi\pi)$ [170]. Results for both the $\Delta I = 3/2$ and 1/2 amplitudes with physical quark masses have been obtained [35–37, 171], the former now including a controlled continuum limit [172]. First results for the CP-violating quantity ϵ' have been obtained [35, 36].

Partial extensions of the formalism above the elastic threshold have been worked out, in particular for the case of multiple two-particle channels [157]. Another theoretical extension is to allow the calculation of form factors between a stable particle and a resonance [173], and between two resonances [174]. The former has been used to calculate the $\gamma\pi \to \rho$ amplitude, albeit for unphysically large quark masses [175, 176], as well as $\gamma K \to K^*$ [177] and $B \to \rho\ell\nu$ [178]. Finally, the formalism for using LQCD to calculate electroweak decays or transitions to three particles, e.g $\gamma^* \to 3\pi$ and $K \to 3\pi$, has recently been worked out [179, 180].

While a systematic extension to decays with many multi-particle channels, e.g., hadronic B decays, has yet to be formulated, a new direction based on smeared spectral functions is being explored [153,181,182]. Correlation functions computed on a Euclidean lattice contain contributions from all states allowed by the symmetry of the inserted operators. Their relative weight depends on their energy E and the time separation t between the operators, and is proportional to e^{-Et}. Correlation functions with different time separations can be combined so as to obtain various desired relative weights between the states [154,183], leading to results for smeared spectral functions, such as the smeared R-ratio [155,184], inclusive hadronic τ decay rates [156,185], inclusive hadron decay rates [186–190], or cross sections [191]. The weight (or the energy-integral kernel) function has to be smooth in order that the construction using correlators with different time separations gives a good approximation. The kernel function required to obtain the inclusive decay rate, for example, does not satisfy this smoothness condition, and one has to introduce some smearing, which has then to be eliminated by taking an appropriate limit. This new source of systematic effect is currently under active investigation [189, 190].

17.2.5 *Status of LQCD simulations*

Until the 1990s, most large-scale lattice simulations were limited to the "quenched" approximation, wherein the fermion determinant is omitted from the path integral. While much of the basic methodology was developed in this era, the results obtained had uncontrolled systematic errors and were not suitable for use in placing precision constraints on the Standard Model. During the 1990s, more extensive simulations including the fermion determinant (also known as simulations with "dynamical" or "sea" quarks) were begun, but with unphysically heavy quark masses ($m_\ell \sim 50-100$ MeV), such that the extrapolation to the physical light quark masses was a source of large systematic errors [196]. During the 2000s, advances in both algorithms and computers allowed simulations to reach much smaller quark masses ($m_\ell \sim 10-20$ MeV) such that LQCD calculations of selected quantities with all sources of error controlled and small became available. Their results played an important role in constraints on the CKM matrix and other phenomenological analyses. In the last decade, simulations directly at the physical isospin-symmetric light quark masses for a range of lattice spacings have become standard, removing the need for a chiral extrapolation and thus significantly reducing the overall error. This has made many lattice QCD results critical for tests of the Standard Model and searches for new physics. Figure 17.3 shows as an example the recent history of improvement in the uncertainty of lattice QCD results for and f_{K^+}/f_{π^+} and $\bar{m}_s(2\text{ GeV})$.

A summary of lattice QCD ensembles produced by some of the international collaborations as of 2024 can be found in Ref. [197]. The present frontier for u/d quarks, as noted above, is the

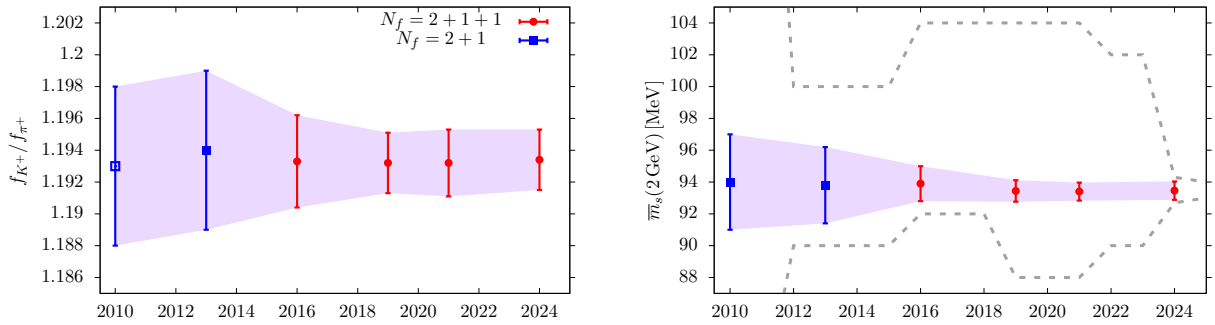

Figure 17.3: History of the FLAG averages of LQCD results for the ratio of kaon and pion decay constants f_{K^+}/f_{π^+} and the strange-quark mass $\bar{m}_s(2\text{ GeV})$ (defined in the $\overline{\text{MS}}$ scheme, μ =2 GeV) [60, 85, 192–195]. In both cases we see a large improvement in the uncertainty over the 14-year timespan—by a factor of 2.5 for f_K^+/f_π^+ (the 2010 result is for the isospin-symmetric f_K/f_π) and a factor of 5 for m_s—as ensemble sizes have grown for improved statistical errors and lattice spacings have become finer and light quark masses closer to the physical point for improved systematic errors. There has also been a shift from $n_f = 2+1$ to $n_f = 2+1+1$ simulations over time. The grey dashed lines for $\bar{m}_s$ indicate the $\pm 1\sigma$ band given in the PDG particle listings (pdglive for 2025). The PDG's evaluation of $\bar{m}_s$ is now in good agreement with the average of the lattice QCD results.

inclusion of isospin breaking. This will be needed to push the accuracy of calculations down to the few tenths of a percent level. For b-quark physics, realistic sea quark content on very fine lattices is needed to push uncertainties down.

On a more qualitative level, analytic and numerical results from LQCD have demonstrated that QCD confines color and spontaneously breaks chiral symmetry. Confinement can be seen as a linearly rising potential between heavy quark and anti-quark in the absence of quark loops. Analytically, this can be shown in the strong coupling limit $g_{\text{lat}} \to \infty$ [1]. At weaker couplings there are precise numerical calculations of the potential that clearly show that this behavior persists in the continuum limit [198–200].

Chiral symmetry breaking was also demonstrated in the strong coupling limit on the lattice [18, 201], and there have been a number of numerical studies showing that this holds also in the continuum limit. The accumulation of low-lying modes of the Dirac operator, which is the analog of Cooper pair condensation in superconductors, has been observed, yielding a determination of the chiral condensate [202–208]. Many relations among physical quantities that can be derived under the assumption of broken chiral symmetry have been confirmed by a number of lattice groups [194].

17.3 Physics applications

In this section we describe the main applications of LQCD that are both computationally mature and relevant for the determination of particle properties.

A general feature to keep in mind is that, since there are many different choices for lattice actions, all of which lead to the same continuum theory, a crucial test is that results for any given quantity are consistent. In many cases, different lattice calculations are completely independent and often have very different systematic errors. Thus, final agreement, if found, is a highly non-trivial check, just as it is for different experimental measurements. Indeed the process of 'blinding' results during analysis, standard in experiment, is being increasingly adopted in lattice calculations to eliminate comparison bias.

The number, variety and precision of the calculations has progressed to the point that an international collaboration, FLAG, has been formed, which aims to collect all lattice results of relevance for a variety of phenomenologically interesting quantities and provide averages of those results that pass appropriate quality criteria. The FLAG averages attempt to account for possible correlations between results (which can arise, for example, if they use common gauge configurations). The most recent FLAG review is from 2024 [85] (see also older editions, Refs. [60, 194, 195, 195]). Our discussion in this section provides summaries for the quantities considered by FLAG, as well as for two topics not discussed by FLAG: the hadron spectrum and the anomalous magnetics moment of the muon. The interested reader can consult the FLAG review for very extensive discussions of the details of the calculations and of the sources of systematic errors.

We stress that the results we quote below are those obtained using the physical complement of light quarks (i.e. $N_f = 2 + 1$ or $2 + 1 + 1$ simulations).

17.3.1 *Spectrum*

The most basic prediction of LQCD is of the hadron spectrum. Once the input parameters are fixed as described in Sec. 17.1.5, the masses or resonance parameters of all other states can be predicted. This includes hadrons composed of light (u, d and s) quarks, as well as heavy-light and heavy-heavy hadrons. It also includes quark-model exotics (e.g., $J^{PC} = 1^{-+}$ mesons) and glueballs. Thus, in principle, LQCD calculations should be able to reproduce many of the experimental results compiled in the Review of Particle Properties. Doing so would test both that the error budgets of LQCD calculations are accurate and that QCD indeed describes the strong interactions in the low-energy domain. The importance of the latter test can hardly be overstated.

What is the status of this fundamental test? As discussed in Sec. 1.2, LQCD calculations are most straightforward for stable, low-lying hadrons. Calculations of the properties of resonances that can decay into two particles are more challenging, but are becoming standard in the meson sector, with the frontier being decays involving baryons. As noted above, the formalism for resonances decaying to three particles exists, but has yet to be applied to resonant channels other than in pioneering calculations. It is also more technically challenging to calculate masses of flavor singlet states (which can annihilate into purely gluonic intermediate states) than those of flavor non-singlets, although again algorithmic and computational advances have begun to make such calculations accessible, including first calculations that reach physical quark masses [209].

The present status for light hadrons is that fully controlled results are available for the masses of the octet light baryons, while results with less than complete control are available for the decuplet baryon resonances, the vector meson resonances and the η and η'. This is discussed in the "Quark Model" review—see, in particular, Fig. 15.9. In addition, it has been possible to calculate the isospin splitting in light mesons and baryons (due to the up-down mass difference and the incorporation of QED). There are also extensive accurate results for heavy-light (D and B systems) and heavy-heavy (ψ, Υ as well as B_c systems). All present results, which are discussed in the "Quark Model" review, are consistent with experimental values, and several predictions have been made. We refer the reader to that review for references to the relevant work.

17.3.2 *Decay constants and bag parameters*

The pseudoscalar meson decay constants can be determined from two-point correlation functions involving the axial-vector current, as discussed in Sec. 17.2.2. The decay constant f_P of a meson P is extracted from the weak matrix element involving the axial-vector current $A_\mu(x)$ using the definition $\langle 0|A_\mu(x)|P(\boldsymbol{p})\rangle = f_P p_\mu \exp(-ip\cdot x)$, where p_μ is the momentum of P and $A_\mu(x)$ is the axial-vector current. (In practice, results with the smallest errors are obtained using the pseudoscalar density operator $P(x) = \bar{q}(x)\gamma_5 q(x)$ instead of $A_\mu(x)$.) Since they are among the simplest quantities to calculate, decay constants provide good benchmarks for lattice methods, in addition to being critical

inputs for the flavor physics phenomenology of leptonic decay rates. Results from several lattice groups for the pion and kaon decay constants now have sub-percent errors. The decay constants in the charm and bottom sectors, $f_{D_{(s)}}$ and $f_{B_{(s)}}$, have also been calculated using the various heavy-quark formulations on the lattice outlined in Sec. 17.1.3. The precision has now reached the sub-percent level for both charmed and bottom mesons, meaning that phenomenological analysis of these leptonic decay rates is limited by the larger experimental uncertainties. Lattice results for all of these decay constants are discussed in detail in the review "Leptonic Decays of Charged Pseudoscalar Mesons." The lattice uncertainty on vector meson decay constants $f_{J/\psi}$ and f_Υ, has also reached ∼1% and the results agree well with the accurate experimental results for the leptonic decay rates of $J/\psi \to \ell^+\ell^-$ and $\Upsilon \to \ell^+\ell^-$ [41,45].

Another important lattice quantity is the kaon bag parameter, B_K, which is needed to turn the precise measurement of CP-violation in kaon mixing into a constraint on the Standard Model. It is defined by

$$\frac{8}{3} m_K^2 f_K^2 B_K(\mu) = \langle \overline{K}^0 | Q_{\Delta S=2}(\mu) | K^0 \rangle, \tag{17.13}$$

where m_K is the kaon mass, f_K is the kaon decay constant, $Q_{\Delta S=2} = \bar{s}\gamma_\mu(1-\gamma_5)d\bar{s}\gamma_\mu(1-\gamma_5)d$ is the four-quark operator of the effective electroweak Hamiltonian and μ is the renormalization scale. The short distance contribution to the electroweak Hamiltonian can be calculated perturbatively, but the hadronic matrix element parameterized by B_K must be computed using non-perturbative methods. In order to be of use to phenomenology, the renormalization factor of the four-quark operator must be matched to a continuum renormalization scheme, e.g., to $\overline{\rm MS}$, as described in Sec. 17.1.6.4. Determinations with percent-level precision using different fermion actions and $N_f = 2+1$ light sea quarks are now available using DWF [210,211], staggered fermions [212], DWF valence on staggered sea quarks [213], and Wilson fermions [11]. The results are all consistent, and the present FLAG average is $\hat{B}_K = 0.7533(91)$ [85] for its renormalization group invariant definition (for original papers, see [11, 211, 213–215]).

The bag parameters for B and B_s meson mixing are defined analogously to that for kaon mixing. The B and B_s mesons contain a valence b-quark so that calculations of these quantities must use one of the methods for heavy quarks described above. Calculations have been done using NRQCD [216, 217], the Fermilab formalism [87], and static heavy quarks [218]. All results are consistent. The FLAG averages for the quantities relevant for B_s and B mixing with $N_f = 2+1$, which are based on results from Refs. [87, 216, 218], are $f_{B_s}\sqrt{\hat{B}_{B_s}} = 274(8)$ MeV and $f_B\sqrt{\hat{B}_B} = 225(9)$ MeV, with their ratio (which is somewhat better determined) being $\xi = 1.206(17)$. There is a single $N_f = 2+1 = 1$ calculation [217] and this gives $f_{B_s}\sqrt{\hat{B}_{B_s}} = 256(6)$ MeV $f_B\sqrt{\hat{B}_B} = 211(6)$ MeV, and $\xi = 1.216(16)$. These are consistent with the $N_f = 2+1$ results at the 2σ level. Errors for quantities involving b quarks are typically larger than those for quantities involving only light quarks, although the difference has steadily decreased in recent years.

For the K, D and B systems, one can also consider the matrix elements of four-fermion operators that arise in beyond-the-standard-model (BSM) theories, which can have a different chiral structure. Knowledge of these matrix elements allows one to constrain the parameters of the BSM theories, and is complementary to direct searches at the LHC. Reliable results are now available from lattice calculations, and are reviewed by FLAG in the case of kaon mixing [85]. Complete results for D and B mixing are presented in Ref. [219, 220] and Ref. [87, 217], respectively.

The results for mixing matrix elements are used in the reviews "The CKM Quark-Mixing Matrix," and "$B^0 - \bar{B}^0$ Mixing."

17.3.3 *Semileptonic form factors*

Semileptonic decay rates can be used to extract CKM matrix elements once the semileptonic form factors are known from lattice calculations.

For example, the matrix element of a pseudoscalar meson P undergoing semileptonic decay to another pseudoscalar meson P' is mediated by the vector current, and can be written in terms of form factors as

$$\langle P'(p')|V_\mu|P(p)\rangle = f_+(q^2)(p+p'-\Delta)_\mu + f_0(q^2)\Delta_\mu\,, \tag{17.14}$$

where $q = p - p'$, $\Delta_\mu = (m_P^2 - m_{P'}^2)q_\mu/q^2$, and V_μ is the quark vector current. Typically, $f_+(q^2)$ dominates the decay rate, since the contribution from $f_0(q^2)$ is suppressed when the final state lepton is light.

For some decays, the shapes of the differential decay rates are well determined by experiment, and, in principle, the values of the form factors are needed from lattice QCD only at some reference value of q^2 in order to extract CKM matrix elements. In these cases, lattice calculations of the form factor shapes may provide further consistency checks or can further improve the precision.

The form factor $f_+(0)$ for $K \to \pi\ell\nu$ decays is highly constrained by the Ademollo-Gatto theorem [221] and chiral symmetry. Old estimates using chiral perturbation theory combined with quark models quote sub-percent precision [222], though they suffer from some model dependence. Utilizing the constraint from the vector current conservation that $f_+(0)$ is normalized to unity in the limit of degenerate up and strange quark masses, the lattice calculation can be made very precise and has now matched the precision of the phenomenological estimates [223–232]. The present FLAG average (from $N_f = 2+1+1$ simulations) is $f_+(0) = 0.9698(17)$ [85], based on Refs. [230, 231].

Charmed meson semileptonic decays have been calculated by different groups using methods similar to those used for charm decay constants, and results are steadily improving in precision [233–238]. Charmed baryon decays have also been computed using a similar method [239, 240].

For semileptonic decays involving a bottom quark, one can use HQET or NRQCD to control the discretization errors from the bottom quark mass at the cost of systematic errors from current renormalisation. Increasingly, calculations are being done with relativistic lattice quark actions and nonperturbative current normalisation. HQET is then used to constrain the extrapolation of the lattice results to the b mass from a range of lower values.

The form factors for the semileptonic decay $B \to \pi\ell\nu$ (and the similar decay $B_s \to K\ell\nu$) have been calculated by a number of groups [241–250]. These B semileptonic form factors are difficult to calculate at low q^2, *i.e.* when the mass of the B-meson must be balanced by a large pion momentum, in order to transfer a large momentum to the lepton pair. The low q^2 region has large discretization errors and very large statistical errors (see signal/noise discussion in Sec. 17.2.2), while the high q^2 region is much more accessible to the lattice. For experiment, the opposite is true. To combine lattice and experimental results it has proved helpful to use the z-parameter expansion [147–150]. This provides a theoretically constrained parameterization of the entire q^2 range, and allows one to obtain $|V_{ub}|$ without model dependence [251]. Analyticity and unitarity can be used to obtain further constraints, including extra information on susceptibilities relevant to the form factors in the time-like region [150, 252–258]. Now that LQCD results for heavy-to-light form factors are available from multiple groups, it has become evident that the results are not always compatible within the quoted errors, suggesting that systematic uncertainties have been underestimated in some cases. Recent fits performed by FLAG to average the form-factor results from different groups have χ^2/d.o.f. substantially larger than 1 and require scale factors [85]. All of the current calculations still involve an extrapolation in the light-quark mass, which is one possible source of underestimated uncertainties. This includes choices made for the form-factor bases used for the extrapolation and the inclusion of poles in the fit functions [250]. Another challenge is

excited-state contamination [143].

The semileptonic decays $B \to D\ell\nu$ and $B \to D^*\ell\nu$ (and the similar decays $B_s \to D_s\ell\nu$ and $B_s \to D_s^*\ell\nu$) can be used to extract $|V_{cb}|$ once the corresponding form factors are known. The lattice calculation is most precise at zero recoil since the bulk of the systematic error cancels for appropriate ratios between $B \to D^{(*)}$ and $B \to B$ or $D^{(*)} \to D^{(*)}$ [259]. Calculations of the $B \to D^{(*)}\ell\nu$ and $B_s \to D_s^{(*)}\ell\nu$ form factors at zero recoil have been performed with various formulations for the heavy quark [260]. Calculations at non-zero recoil momenta have also been performed to constrain the functional form of the form factor, which can be used to extrapolate the experimental data to the zero-recoil point or to determine $|V_{cb}|$ directly at the non-zero recoil points [42, 261–266]. The range of q^2 that can be handled for B-meson decays in lattice QCD is growing as more accurate results become available on finer lattices. Comparison of the shape of the form factors between lattice calculations and experiments provides non-trivial cross-checks.

Semileptonic decays of the Λ_b baryon can also be used to constrain $|V_{cb}|$ and $|V_{ub}|$ using lattice calculations of the relevant form factors [267]. Another process sensitive to $|V_{ub}|$ is $B \to \rho\ell\nu$, which is more challenging for lattice QCD due to the unstable nature of the ρ resonance. A first calculation of the $B \to \pi\pi\ell\nu$ P-wave form factors and the resulting $B \to \rho\ell\nu$ resonance form factors, using the finite-volume formalism for $\pi\pi$ scattering as discussed in Sec. 17.2.4 has recently been completed, but so far only at a heavier-than-physical pion mass [178].

Rare decays such as $B \to K\ell^+\ell^-$ involve local matrix elements similar to those needed for charged-current semileptonic decays, Eq. (17.14), as well as nonlocal matrix elements, which, for example, involve the decay chain $b \to sc\bar{c} \to s\ell^+\ell^-$. Except for rare kaon and hyperon decays [268–270], only the local matrix elements have been calculated on the lattice (see, however, Ref. [271] for a possible strategy and exploratory steps to compute $b \to sc\bar{c} \to s\ell^+\ell^-$ on the lattice). In the phenomenology of $b \to s\ell^+\ell^-$ decays, the nonlocal matrix elements are currently treated using continuum methods such as operator product expansions and light-cone sum rules, and the intermediate q^2 region where $c\bar{c}$ resonances are present must be avoided. Recent lattice calculations for $b \to s\ell^+\ell^-$ decays [245, 272, 273] suggest some tension with the experimentally observed decay rates, but systematic errors, including those from the approximations used for the nonlocal matrix elements, need to be carefully studied before drawing any definite conclusions. A similar study for the baryonic decay mode $\Lambda_b \to \Lambda\ell^+\ell^-$ can be found in Ref. [274].

The results discussed in this section are used in the reviews "The CKM Quark-Mixing Matrix," "V_{ud}, V_{us}, the Cabibbo Angle and CKM Unitarity," and "Semileptonic b-hadron decays, determination of V_{cb}, V_{ub}."

17.3.4 *Long-distance contributions to weak-interaction processes*

There are other hadronic processes, for which long-distance contributions are important, where lattice calculations can significantly improve our quantitative understanding.

One example is the long-distance contribution to the neutral kaon mass splitting, ΔM_K. This requires the evaluation of a four-point function, constructed from the two-point functions described in Sec. 17.2.2 by the insertion of two electroweak Hamiltonians [275, 276]. Another example is the long-distance contribution to ϵ_K, which provides a correction to the contribution of the mixing parameter B_K [277]. Rare kaon decays $K \to \pi\ell^+\ell^-$ and $K \to \pi\nu\bar{\nu}$ also include long-distance contributions, and their lattice calculations are discussed in [268, 269]. Related processes $\pi^0 \to e^+e^-$ [278] and $K_L \to \mu^+\mu^-$ [279] have also been studied.

Radiative leptonic decays $\pi \to \ell\nu\gamma^{(*)}$, $K \to \ell\nu\gamma^{(*)}$, and $D \to \ell\nu\gamma^{(*)}$ also include two operator insertions, i.e. an electroweak Hamiltonian and an electromagnetic current, and similar techniques developed for the rare decays above can be applied [64, 280].

We note that similar lattice methods allow the calculation of the γW box contribution to the

radiative corrections to semileptonic decays of pions and kaons [281]. The extension to neutron β decay is an important next step, as this promises to reduce the theoretical uncertainty in the extraction of $|V_{ud}|$ from neutron decays [282].

17.3.5 *Strong gauge coupling*

As explained in Sec. 17.1.5.1, for a given lattice action, the choice of bare lattice gauge coupling, $g_{\rm lat}$, determines the lattice spacing a. If one then calculates a as described in Sec. 17.1.5.1, one knows the strong gauge coupling in the bare lattice scheme at the scale $1/a$, $\alpha_{\rm lat} = g^2_{\rm lat}/(4\pi)$. This is, however, not useful for comparing to results for α_s obtained from other inputs, such as deep inelastic scattering or jet shape variables, because the latter results give α_s in the $\overline{\rm MS}$ scheme, which is commonly used in such analyses, and the conversion factor between the lattice and $\overline{\rm MS}$ schemes is known to converge poorly in perturbation theory [283]. Instead, one must use a method that directly determines α_s on the lattice in a scheme closer to $\overline{\rm MS}$.

Several such methods have been used, all following a similar strategy. One calculates a short-distance quantity K both perturbatively ($K^{\rm PT}$) and non-perturbatively ($K^{\rm NP}$) on the lattice, and requires equality: $K^{\rm NP} = K^{\rm PT} = \sum_{i=0}^{n} c_i \alpha_s^i$. Solving this equation one obtains α_s at a scale related to the quantity being used. Often, α_s thus obtained is not defined in the conventional $\overline{\rm MS}$ scheme, and one has to convert among the different schemes using perturbation theory. Unlike for the bare lattice scheme, the required conversion factors are reasonably convergent. As a final step, one uses the renormalization group to run the resulting coupling to a canonical scale (such as M_Z). In each step described above a key systematic error comes from the truncation of the perturbative expansion. This error must be estimated carefully, for example using data-driven methods.

In the work of the HPQCD collaboration [284, 285], the short-distance quantities are Wilson loops of several sizes and their ratios. These quantities are perturbatively calculated through $\mathcal{O}(\alpha_s^3)$ using the V-scheme defined through the heavy quark potential. The coefficients of even higher orders are estimated using the data at various values of a. In addition, this work obtains a result for α_s by matching with $\alpha_{\rm lat}$ in a tadpole-improved scheme that improves convergence.

Another choice of short-distance quantities is to use current-current correlators. Appropriate moments of these correlators are ultraviolet finite, and by matching lattice results to the *continuum* perturbative predictions, one can directly extract the $\overline{\rm MS}$ coupling [286]. The method can be applied for light meson correlators [287–290] as well as heavy meson correlators [40, 285, 291–294]. Yet another choice of short-distance quantity is the static-quark potential, where the lattice result for the potential is compared to perturbative calculations; this method was used to compute α_s within 2+1 flavor QCD [295–300]. There is also a determination of α_s from a comparison of lattice data for the ghost-gluon coupling with that of perturbation theory [301, 302].

With a definition of α_s given using the Schrödinger functional, one can non-perturbatively control the evolution of α_s to high-energy scales, such as 100 GeV, where the perturbative expansion converges very well and essentially no truncation error remains in the matching to the $\overline{\rm MS}$ scheme. This step-scaling method developed by the ALPHA collaboration [106] has been applied to 2+1-flavor QCD in [303–305]. We also note that the gradient-flow coupling [306] is employed at low-energies in [84, 305] to avoid large statistical errors associated with the Schrödinger functional coupling. An alternative path to determine the QCD Λ parameter for three flavors, $\Lambda^{(3)}$, from that of the quenched theory, $\Lambda^{(0)}$, has also been developed [307]. This approach aims to benefit from the fact that quenched theories are much faster to simulate. The matching between different flavors can be performed accurately at sufficiently high energy scales.

The various lattice methods for calculating α_s have significantly different sources of systematic error. The FLAG review [85] reports an estimate $\alpha^{(5)}_{\overline{\rm MS}}(M_Z) = 0.1183(7)$, based on Refs. [285, 290, 292, 300, 303, 305, 308–311]. A comparison to other phenomenological determinations can be found

in the "Quantum Chromodynamics" review, where it is clear that the uncertainty in the LQCD average is smaller than that from other approaches. Since $\sigma_{\alpha_s} < \mathcal{O}(\alpha_s^3)$, high-order perturbative series are needed to take advantage of further improvements in uncertainty.

17.3.6 *Quark masses*

The quark mass parameters in the lattice QCD action are well-defined running masses, but they need to be converted into masses in a conventional scheme at a canonical scale, such as $\overline{\text{MS}}$ at 2 or 3 GeV, to be useful in continuum phenomenology such as the prediction of Higgs decay rates. This conversion requires multiplication by a finite renormalisation constant, which depends on the quark action. Older calculations determined the renormalisation constant using low-order lattice perturbation theory. Most recent calculations use instead an intermediate NPR method (e.g., RI/MOM or RI/SMOM, see Sec. 17.1.6.4) which can be applied by numerical calculation on the lattice and which is then converted to the $\overline{\text{MS}}$ scheme using three-loop continuum perturbation theory (see, e.g., [41, 210, 312–315]). Alternatively, using a definition based on the Schrödinger functional, the quark mass can be evolved to a high scale non-perturbatively [316, 317], before applying perturbative matching to the $\overline{\text{MS}}$ scheme; this minimises the perturbative matching uncertainties. Further approaches are available for heavy quarks. These include matching current-current correlators at short distances calculated on the lattice to those obtained in continuum perturbation theory in the $\overline{\text{MS}}$ scheme [40, 104, 285, 291, 292, 294], or using HQET mass relations matched to $\overline{\text{MS}}$ either via a ratio method [318] or using the intermediate minimal renormalon-subtracted scheme [319, 320].

The accuracy of lattice QCD determinations of quark masses—uncertainties range from 2–4% for u quark (at a scale of 2 GeV) down to 0.3% for the b quark (at a scale equal to its mass) [85]—mean that they dominate the values given in the Particle Listings, particularly for u, d and s quarks (see right-hand plot of Fig. 17.3). As discussed in Secs. 17.1.5.2 and 17.1.5.3, the tuning of lattice quark masses uses meson masses that are known to sub-MeV precision experimentally and have no signal/noise issues in lattice QCD (see Sec. 17.2.2). Uncertainties coming from the value of the lattice spacing that might otherwise limit precision are also suppressed for heavy quarks because of the relationship between quark and meson masses [292]. A further key point is that ratios of lattice masses using the same quark action are equal in the continuum limit to the ratio of $\overline{\text{MS}}$ masses at a given scale, since renormalisation constants cancel in QCD. The ratio m_c/m_s has been calculated to 0.2% [44] and m_b/m_c to 0.3% [44, 77] and these ratios can be used to "cascade" the accuracy of heavy quark masses down to light quark masses [44, 292]. When the effect of the quark's electric charge is included, mass ratios between up-type and down-type quarks are no longer scale-invariant and must be determined at a specific scale [73, 75, 77, 321]. Lattice QCD calculations are now accurate enough to discern QED effects. The ratio m_b/m_c needed for the calculation of $\Gamma(H \to b\bar{b})/\Gamma(H \to c\bar{c})$ runs from 4.586(12) at a scale of 3 GeV [77] to 4.607(12) at m_H, nearly 2σ higher, for example.

Results are summarized in the review of "Quark Masses."

17.3.7 *The anomalous magnetic moment of the muon*

A notable success for LQCD has been the determination of the QCD contributions to the anomalous magnetic moment of the muon, a_μ, in the Standard Model [323], for comparison to recent experimental results from the Muon $g-2$ experiment [322]. This comparison (see Fig. 17.4) now yields $a_\mu^{\text{expt.}} - a_\mu^{\text{SM}} = 39(64) \times 10^{-11}$, showing agreement between experiment and the SM at the level of 550 ppb. The uncertainty is dominated by that from theory (the experimental uncertainty is 124 ppb), and in particular by that from the largest QCD contribution known as the leading-order hadronic vacuum polarization (LO-HVP). Here we describe briefly how the lattice QCD calculations for a_μ^{SM} are done, giving a little more detail than on other topics covered in this review to reflect the size of the community effort involved and the timeliness of the results. For a

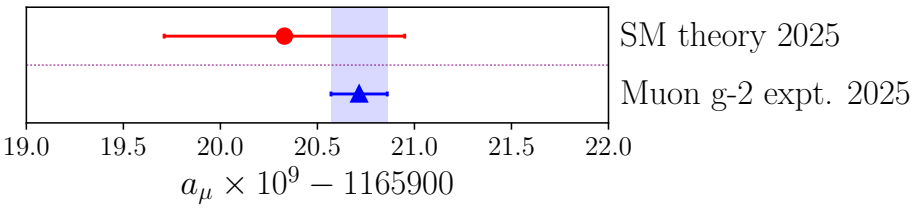

Figure 17.4: The current status of a_μ, comparing the experimental world average [322] with SM theory using lattice QCD for the largest, LOHVP, QCD contribution combined with QED, electroweak and other QCD contributions [323].

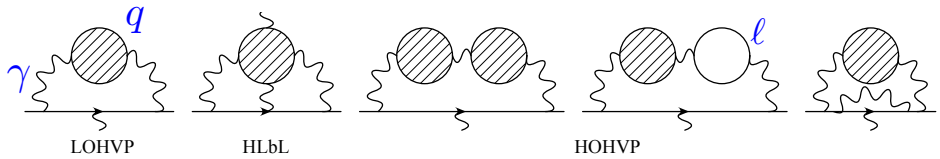

Figure 17.5: QCD contributions to a_μ. From left to right: the leading-order hadronic vacuum polarisation (LOHVP), hadronic light-by-light (HLbL), higher-order HVP (HOHVP). The horizontal lines represent the μ and wiggly lines are photons, with the vertical photon the B field probing the muon magnetic moment. Hatched loops are strongly-interacting and formed from $\gamma^* \to q\overline{q} \to \gamma^*$; open loops are lepton loops. Figure from [324].

recent review see [325].

The anomalous magnetic moment $a_\mu = (g-2)/2$ quantifies the 0.1% impact on the muon magnetic moment from the fact that the muon is embedded in a quantum field theory and can therefore interact directly and indirectly with all the SM particles (and BSM particles, if they exist). In the SM the muon can, for example, emit a virtual photon that generates for an instant a quark-antiquark pair before they are re-absorbed as a photon (see Fig. 17.5). The quark-antiquark "bubble" produced here is strongly-interacting. Because the relevant energy scale is a low one, set by the muon mass, determining the effect of the bubble on a_μ requires a fully nonperturbative QCD calculation. This LO-HVP contribution is straightforward to calculate in lattice QCD. It requires the same two-point correlation function $C_{XY}(t, \boldsymbol{p}=0) = \sum_{\boldsymbol{x}} \langle O_X(t,\boldsymbol{x}) O_Y^\dagger(0)\rangle$ (see Sec. 17.2.2) used to determine the spectrum of flavor-diagonal vector mesons (because O here is the QED current that couples to the photon). Instead of fitting $C_{XY}(t)$ as a function of time separation, t, between O_X and O_Y to isolate specific states, here $C_{XY}(t)$ is multiplied by a kernel function, $K(t)$, and summed over all t (and therefore all states) to obtain the LO-HVP contribution [326,327]. The challenge in doing this comes from the need to achieve very high accuracy. Vector-vector correlation functions suffer from exponentially falling signal/noise as t increases (see Sec. 17.2.2) and this is particularly problematic for the correlation functions constructed from u and d quark fields that yield 90% of the LO-HVP. In the u/d case the LO-HVP time-sum has a more significant contribution from large t than for heavier quarks and the signal/noise problem is worse, making it harder to achieve good statistical accuracy. A further issue is that of the finite-volume of the lattice. Although the u/d correlation function is dominated by the ρ meson, the lowest-energy ground-state, which starts to be significant at large t values, is made of two pions. These light long-wavelength particles can 'see' the lattice boundary, generating finite-volume effects that must be corrected using ChPT or other

methods.

As well as calculating the LO-HVP contribution in the continuum and chiral limits from the vector-vector correlation for each quark flavor as described above, additional small corrections must be determined from quark-line disconnected correlation functions, from QED and from $m_u \neq m_d$ effects. The first complete LQCD calculation of the LO-HVP contribution appeared in 2020 from the BMW collaboration with sub-percent uncertainty [328]. Since then multiple LQCD collaborations have obtained accurate results for different pieces of the LO-HVP allowing stringent comparisons between them and enabling a strong consensus to be obtained on the result. A particularly useful approach has been to determine the LO-HVP in a "time-window" on the lattice [327, 329]. By summing over a time range that cuts out large t values, both the statistical and systematic uncertainties can be improved. Eight different groups using six different quark actions have each achieved between 0.2% and 1% precision for u/d quarks with $m_u = m_d$ in a time window from 0.4 to 1.0 fm (with rounded edges of width 0.15 fm) [328, 330–337]. The striking agreement between the results (most of which were 'blinded' during analysis) represents one of the best tests of LQCD that has been done.

The 2025 White Paper from the Muon $g-2$ Theory Initiative [323] quotes an average value for the LO-HVP from lattice QCD of $713.2(6.1) \times 10^{-11}$ [328–334, 336–345]. It is this value, added to the other contributions to $a_\mu^{\rm SM}$, that yields the SM theory result in agreement with experiment quoted above and shown in Fig. 17.4 (and dominates its uncertainty). Note that the 2025 LO-HVP value is larger than that in the 2020 White Paper [346] by 2.8σ. The earlier value was obtained using a 'data-driven' approach in which experimental data for the cross-section for $e^+e^- \to$ hadrons as a function of the centre-of-mass energy, $\sqrt{s}$, are converted using analyticity and the optical theorem into values for the hadronic vacuum polarisation function. The first hints of tension between LQCD and the data-driven value came in 2020 [328] and this has become more significant with the LQCD focusing on time-windows, since a disagreement in any time-window is sufficient to demonstrate a disagreement in the underlying hadronic vacuum polarisation function. The lattice LO-HVP value from the 0.4–1.0 fm window [323] now disagrees with that from the data-driven approach using pre-2020 experimental data [347] by 5σ. The channel which contributes most to the data-driven LO-HVP is $e^+e^- \to \pi^+\pi^-$ at low values of $\sqrt{s} < 1$ GeV^2. New values for this cross-section from the CMD3 collaboration in 2023 [348] are higher than previous results and in tension with them so that a combination has not proved possible. LQCD favors the CMD3 results.

A quantity linked to the LO-HVP is the hadronic contribution to the running of the QED coupling since both depend on the hadronic vacuum polarization function. In tandem with LO-HVP calculations, some lattice groups have calculated $\Delta\alpha_{\rm had}$ for a range of spacelike momenta, $Q^2 < 10$ GeV^2. Again, tension is seen at these Q^2 values with the pre-2020 data-driven results but the tension is much diminished on translating the results to the scale M_Z so that both agree with global EW fit values for $\Delta\alpha_{\rm had}(M_Z^2)$ [328, 349].

Along with the resolution of the issues in the experimental e^+e^- data, future progress on the LO-HVP will require reduced uncertainty from lattice QCD; an uncertainty on the SM a_μ comparable to that of the experiment will require the LO-HVP to be determined to 0.2%. This may need a combination of lattice QCD and data-driven approaches in complementary time-windows [337,350].

The LO-HVP contribution to $a_\mu^{\rm SM}$ appears at $\mathcal{O}(\alpha^2)$. QCD contributions at $\mathcal{O}(\alpha^3)$ are about 70 times smaller and include higher-order HVP pieces as well as a diagram in which a quark bubble is connected to four photons. This is known as the hadronic light-by-light (HLbL) contribution (see Fig. 17.5). Although small, it must be determined to 10% accuracy to reach the uncertainty aim for $a_\mu^{\rm SM}$. Three LQCD groups employing different quark actions have performed direct calculations of the HLbL contribution, using a number of ingenious methods to handle the four-point correlation functions needed [351–355]. Good agreement is found and the 2025 White paper averages them to

give $122.5(9.0) \times 10^{-11}$ as the HLbL contribution to a_μ. LQCD calculations are also being done to provide hadronic input to the phenomenological framework for determining the HLbL contribution. The most important of these are the transition form factors, $F_{P\gamma^*\gamma^*}(q_1^2, q_2^2)$ for pseudoscalar (π^0, η, η' etc.) meson exchange. The form factor calculation requires three-point correlation functions with a weighted sum over the time separation of the two photons to fix the (spacelike) photon virtualities. At $q_1^2 = q_2^2 = 0$ the π^0 form factor yields $\Gamma(\pi^0 \to \gamma\gamma)$ and the π^0 lifetime, for comparison to experiment. Four lattice groups using four different quark actions have calculated the π^0 pole contribution to the HLbL with good agreement [356–359]. Overall the phenomenological approach to the HLbL gives a total result in agreement with the direct lattice QCD value within 2σ, allowing a reliable combination with an uncertainty of 8.5% [323], nearly a factor of 2 improvement over that in 2020 [346] and now at the level needed.

17.3.8 *Nucleon structure*

Another topic under active investigation is nucleon structure. Matrix elements of local currents, $\langle N(P', s')|J|N(P, s)\rangle$, can be computed on the lattice using techniques similar to those used for meson semileptonic decays. Some of the challenges involved are the rapid degradation of the signal-to-noise ratio of correlation functions, behaving like $e^{-(E_N - 3m_\pi/2)t}$ as a function of the Euclidean time separation [131] (this generalizes the result given in Sec.17.2.2 to moving nucleons with energy $E_N(P)$), excited-state contamination at finite t, such as those from nearby nucleon-pion states [360], and additional sources of statistical noise for quark-disconnected contractions and gluonic currents. In matrix elements of isovector quark currents, the disconnected contributions cancel for $m_u = m_d$. The isovector axial charge, which corresponds to a zero-momentum matrix element of the axial current, has been calculated on the lattice with 1%-level precision [361]. The latest results for the axial, scalar, and tensor charges of the nucleon—both isovector and flavor-diagonal—are reviewed by FLAG [85]. Introducing a nonzero momentum transfer, one can extract form factors in much the same way. Lattice calculations of the electromagnetic form factors are approaching the precision needed to compare with the experimental data on ep scattering; see, e.g., Refs. [362, 363]. The axial form factors play a crucial role in the estimate of the expected event rate in the current and future neutrino experiments, such as T2K and DUNE, and lattice calculations are also reaching the required precision, as reviewed in Ref. [364].

Moving beyond matrix elements of local currents, of particular interest for collider physics are parton structure functions and parton distribution functions. Their experimental determination is discussed in the "Structure Functions" section of the Review of Particle Properties. Lattice calculations increasingly contribute to the knowledge of these quantities, using methods described in the following; see [365] for a recent review. Here we provide a brief summary.

The partonic structure functions of nucleon are defined through the hadronic tensor $W_{\mu\nu}(q, \nu) = \frac{1}{4\pi} \int d^4z\, e^{iqz} \langle N(P)|[J_\mu^\dagger(z), J_\nu(0)]|N(P)\rangle$ for a nucleon state $|N(P)\rangle$ with four-momentum P. It becomes a function of $x = Q^2/2M\nu$ ($Q^2 \equiv -q^2$ and $\nu = q \cdot P/M$ with M the nucleon mass) in the limit of Q^2 and $\nu \to \infty$ (Bjorken scaling). In this kinematical limit, the two inserted currents $J_\mu^\dagger(z)$ and $J_\nu(0)$ are separated nearly on the light-cone, and its direct computation on the Euclidean lattice is ill-defined. Instead, one can use OPE to represent the current product in terms of local operators, for which the lattice calculation becomes possible at least for the lowest orders of the OPE, which corresponds to an expansion in $1/Q^2$ (or in terms of twist, strictly speaking). For example, the lowest-order moment $\langle x \rangle$ is a matrix element of operators of the form $\bar{q}\gamma_\mu D_\nu q$, and it provides an x-moment of the structure function. (There are different quantities depending on flavour and spin compositions.) Currently available results are summarized in the FLAG review [85]. Lattice calculations of higher moments are complicated by power divergences; methods to avoid this issue have been proposed in, e.g., Refs. [366–368] and are being implemented.

There are also methods that attempt to directly obtain the x-dependence of the Parton Distribution Functions (PDF) rather than their x-moments. One possibility is to compute the temporal Fourier transformation of $W_{\mu\nu}(q,\nu)$, which is a function of spatial momenta $\boldsymbol{P}$, $\boldsymbol{q}$ and the time separation τ between the currents [369]. It contains contributions from all possible states generated between the currents with a factor $e^{-q^0\tau}$, and the ν dependence (or q^0 dependence in the rest frame of the N) can be reproduced if one can invert the Laplace transform using techniques like the Backus-Gilbert method [153] and its variant [154] or the Maximum Entropy Method [370,371]. This reconstruction is, however, an example of the infamous inverse problem and no general solution is known. The methods being studied are closely related to those being developed for calculating inclusive decay rates; see Sec. 17.2.4. The problem may be circumvented if one is interested in the hadronic tensor in a different kinematical setup, e.g. the Compton amplitude, for which q^0 is too small to produce any real hadronic states between the two currents [367]. The Compton amplitude can be written using a Cauchy integral of the hadronic tensor with physical kinematics, so that some constraints can be obtained for the structure functions.

The approach proposed by Ji [372] treats a matrix element of the form $\langle N(P)|\bar{q}(z)\gamma_\mu W(0,z)\cdot q(0)|N(P)\rangle$ with a Wilson line $W(0,z)\equiv\exp[ig\int_0^z dz' A_z(z')]$ connecting the quark fields separated in spatial z-direction on the lattice. The result can be related to PDF in the limit of large $\boldsymbol{P}$. The method is under active theoretical study including the renormalization of the non-local operator as well as the necessity of large momentum. The large momentum limit can be approached with the help of the Large Momentum Effective Theory [373]. See [365], for more details.

The signal-to-noise problem mentioned earlier becomes even more severe for large-momentum nucleon states. Several techniques have been introduced to improve the signal by modifying the interpolating operator to produce the nucleon state, including momentum-smearing [374] and the use of kinematically enhanced gamma structures [375].

More details of nucleon structure can be probed by determining Generalized Parton Distributions (GPDs), through which one can obtain the angular momentum distributions of partons. Another way to study the three-dimensional structure of the nucleon is to determine Transverse Momentum-dependent Distributions (TMDs). Developing methods to calculate these quantities is an active research area; for a recent review, see [376–378], for example. Two key ingredients in determinations of TMDs are the so-called soft function and the Collins-Soper kernel; both can be computed on the lattice [379].

Finally, we note that there are ongoing lattice calculations of the nucleon electric dipole moments caused by a nonzero value of $\theta_{\rm QCD}$ or by BSM physics; see, for example, Ref. [380] for a recent review.

17.3.9 *Other applications of lattice QCD*

In this review we have concentrated on applications of LQCD that are relevant to the quantities discussed in the Review of Particle Properties. We have not considered at all several other applications that are being actively pursued by simulations. Here we list the major such applications. The reader can consult the aforementioned texts [2–4] for further details, as well as the proceedings of recent lattice conferences [381], and several recent white papers [382,383]

LQCD can be used, in principle, to simulate QCD at non-zero temperature and density, and in particular to study how confinement and chiral-symmetry breaking are lost as T and μ (the chemical potential) are increased. It is found that, for the physical values of the quark masses, the deconfinement and chiral-symmetry-restoration transitions are smooth crossovers, rather than phase transitions, and that they occur together. This is of relevance to heavy-ion collisions, the early Universe and neutron-star structure. In practice, finite-temperature simulations are computationally tractable and relatively mature, while simulations at finite μ suffer from a "sign problem"

and are at a less developed stage.

Finally, we note that there is much recent interest in studying QCD-like theories with more fermions, possibly in other representations of the gauge group (see, e.g., [383, 384]). The main interest is to find nearly-conformal theories which might be candidates for "walking technicolor" models.

17.4 Outlook

While LQCD calculations have made major strides in the last decade, and are now playing a key role in constraining the Standard Model, there are many calculations that could be done in principle but are not yet mature due to limitations in computational resources. As we move to exascale resources (10^{18} floating point operations per second), the list of mature calculations will grow. In the longer term, LQCD may be able to harness the power of quantum computers, including their potential for new types of calculation. How to do this is an active area of study, see, for example [385].

Examples of calculations that we expect to mature in the next few years are results for B meson and Λ_b baryon form factors covering the full range of q^2 (see Sec.17.3.3); results for excited hadrons, including quark-model exotics, at close to physical light-quark masses; results for structure functions and related parton distribution functions (see Sec.17.3.8); results for a variety of nucleon matrix elements; $\pi \to \gamma\gamma$ and related amplitudes; long-distance contributions to $\overline{K} \leftrightarrow K$ mixing and rare kaon decays such as $K \to \pi\nu\bar{\nu}$; and results for inclusive decay rates (see Sec.17.2.4). There will also be steady improvement in the precision attained for the mature quantities discussed in previous sections. For example, an improvement of a factor of 2 in the uncertainty of QCD contributions to a_μ is required for better alignment with the experimental uncertainty (see Sec. 17.3.7). The detailed error budgets that accompany many lattice QCD calculations make it possible to see what area needs improvement for future precision gains and to judge what gains may be possible.

17.5 Acknowledgments

We are grateful to David Lin and Alejandro Vaquero for comments and suggestions.

References

[1] K. G. Wilson, Phys. Rev. **D10**, 2445 (1974).

[2] T. Degrand & C. DeTar, "Lattice Methods for Quantum Chromodynamics," World Scientific (2006).

[3] C. Gattringer & C.B. Lang, "Quantum Chromodynamics on the Lattice: An Introductory Presentation," Springer (2009).

[4] "Modern Pespectives in Lattice QCD: quantum field theory and high performance computing" (Lecture notes of the Les Houches Summer School, Vol. 93) eds. L. Lellouch *et al.*, Oxford Univ. Press. (Aug. 2011).

[5] W. Zimmermann, in "Lectures on Elementary Particles and Quantum Field Theory", ed. S. Deser et al., MIT Press, Cambridge, MA (1971); K. Symanzik, Nucl. Phys. **B226**, 187 (1983); K. Symanzik, Nucl. Phys. **B226**, 205 (1983).

[6] M. Lüscher and P. Weisz, Commun. Math. Phys. **97**, 59 (1985), [Erratum: Commun. Math. Phys. 98, 433(1985)].

[7] Y. Iwasaki (1983), UT-HEP-118, [arXiv:1111.7054].

[8] H. B. Nielsen and M. Ninomiya, Phys. Lett. **105B**, 219 (1981).

[9] B. Sheikholeslami and R. Wohlert, Nucl. Phys. **B259**, 572 (1985).

[10] K. Jansen *et al.*, Phys. Lett. **B372**, 275 (1996), [hep-lat/9512009].

[11] S. Dürr *et al.*, Phys. Lett. B **705**, 477 (2011), [arXiv:1106.3230].

[12] N. Ishizuka *et al.*, Phys. Rev. **D92**, 7, 074503 (2015), [arXiv:1505.05289].

[13] A. Francis *et al.*, Comput. Phys. Commun. **255**, 107355 (2020), [arXiv:1911.04533].

[14] R. Frezzotti *et al.* (Alpha), JHEP **08**, 058 (2001), [hep-lat/0101001].

[15] R. Frezzotti and G. C. Rossi, JHEP **08**, 007 (2004), [hep-lat/0306014].

[16] R. Frezzotti and G. C. Rossi, Nucl. Phys. Proc. Suppl. **128**, 193 (2004), [hep-lat/0311008].

[17] R. Frezzotti and G. C. Rossi, JHEP **10**, 070 (2004), [hep-lat/0407002].

[18] L. Susskind, Phys. Rev. **D16**, 3031 (1977); N. Kawamoto and J. Smit, Nucl. Phys. B **192**, 100 (1981); H. S. Sharatchandra, H. J. Thun and P. Weisz, Nucl. Phys. B **192**, 205 (1981).

[19] M. Golterman, PoS **CONFINEMENT8**, 014 (2008), [arXiv:0812.3110].

[20] C. Bernard, Phys. Rev. **D73**, 114503 (2006), [hep-lat/0603011]; S. R. Sharpe, PoS **LAT2006**, 022 (2006), [hep-lat/0610094].

[21] J. A. Bailey, Phys. Rev. D **75**, 114505 (2007), [hep-lat/0611023]; Y. Lin *et al.*, Phys. Rev. D **103**, 5, 054510 (2021), [arXiv:2010.10455].

[22] G. P. Lepage, Phys. Rev. **D59**, 074502 (1999), [hep-lat/9809157].

[23] A. Bazavov *et al.* (MILC), Rev. Mod. Phys. **82**, 1349 (2010), [arXiv:0903.3598].

[24] E. Follana *et al.* (HPQCD, UKQCD), Phys. Rev. **D75**, 054502 (2007), [hep-lat/0610092].

[25] C. T. H. Davies *et al.*, Phys. Rev. **D82**, 114504 (2010), [arXiv:1008.4018].

[26] C. McNeile *et al.*, Phys. Rev. **D85**, 031503 (2012), [arXiv:1110.4510].

[27] G. C. Donald *et al.*, Phys. Rev. **D86**, 094501 (2012), [arXiv:1208.2855].

[28] P. H. Ginsparg and K. G. Wilson, Phys. Rev. **D25**, 2649 (1982).

[29] P. Hasenfratz, V. Laliena and F. Niedermayer, Phys. Lett. **B427**, 125 (1998), [hep-lat/9801021].

[30] M. Lüscher, Phys. Lett. **B428**, 342 (1998), [hep-lat/9802011].

[31] D. B. Kaplan, Phys. Lett. **B288**, 342 (1992), [hep-lat/9206013]; Y. Shamir, Nucl. Phys. **B406**, 90 (1993), [hep-lat/9303005]; Y. Shamir, Nucl. Phys. **B417**, 167 (1994), [hep-lat/9310006].

[32] H. Neuberger, Phys. Lett. **B417**, 141 (1998), [hep-lat/9707022]; H. Neuberger, Phys. Lett. **B427**, 353 (1998), [hep-lat/9801031].

[33] A. Borici, NATO Sci. Ser. C **553**, 41 (2000), [hep-lat/9912040].

[34] A. D. Kennedy (2006), [hep-lat/0607038].

[35] Z. Bai *et al.* (RBC, UKQCD), Phys. Rev. Lett. **115**, 21, 212001 (2015), [arXiv:1505.07863].

[36] R. Abbott *et al.* (RBC, UKQCD), Phys. Rev. D **102**, 5, 054509 (2020), [arXiv:2004.09440].

[37] T. Blum *et al.* (2023), [arXiv:2306.06781].

[38] E. Shintani *et al.* (JLQCD), Phys. Rev. Lett. **101**, 242001 (2008), [arXiv:0806.4222].

[39] P. A. Boyle *et al.*, JHEP **12**, 008 (2017), [arXiv:1701.02644].

[40] K. Nakayama, B. Fahy and S. Hashimoto, Phys. Rev. **D94**, 5, 054507 (2016), [arXiv:1606.01002].

[41] D. Hatton *et al.* (HPQCD), Phys. Rev. D **102**, 5, 054511 (2020), [arXiv:2005.01845].

[42] J. Harrison and C. T. H. Davies (HPQCD), Phys. Rev. D **105**, 9, 094506 (2022), [arXiv:2105.11433].

[43] A. Bazavov *et al.*, Phys. Rev. **D98**, 7, 074512 (2018), [arXiv:1712.09262].

[44] A. Bazavov *et al.* (Fermilab Lattice, MILC, TUMQCD), Phys. Rev. **D98**, 5, 054517 (2018), [arXiv:1802.04248].

[45] D. Hatton *et al.*, Phys. Rev. D **103**, 5, 054512 (2021), [arXiv:2101.08103].

[46] E. Eichten and B. R. Hill, Phys. Lett. **B234**, 511 (1990).

[47] J. Heitger and R. Sommer (ALPHA), JHEP **02**, 022 (2004), [hep-lat/0310035]; B. Blossier *et al.* (ALPHA), JHEP **12**, 039 (2010), [arXiv:1006.5816].

[48] B. A. Thacker and G. P. Lepage, Phys. Rev. **D43**, 196 (1991); G. P. Lepage *et al.*, Phys. Rev. **D46**, 4052 (1992), [hep-lat/9205007].

[49] R. J. Dowdall *et al.* (HPQCD), Phys. Rev. **D85**, 054509 (2012), [arXiv:1110.6887].

[50] A. X. El-Khadra, A. S. Kronfeld and P. B. Mackenzie, Phys. Rev. **D55**, 3933 (1997), [hep-lat/9604004].

[51] S. Aoki, Y. Kuramashi and S.-i. Tominaga, Prog. Theor. Phys. **109**, 383 (2003), [hep-lat/0107009].

[52] N. H. Christ, M. Li and H.-W. Lin, Phys. Rev. **D76**, 074505 (2007), [hep-lat/0608006].

[53] Y. Aoki *et al.* (RBC, UKQCD), Phys. Rev. **D86**, 116003 (2012), [arXiv:1206.2554].

[54] N. H. Christ *et al.*, Phys. Rev. **D91**, 5, 054502 (2015), [arXiv:1404.4670].

[55] M. B. Oktay and A. S. Kronfeld, Phys. Rev. **D78**, 014504 (2008), [arXiv:0803.0523].

[56] J. A. Bailey *et al.*, Eur. Phys. J. **C77**, 11, 768 (2017), [arXiv:1701.00345].

[57] B. Blossier *et al.* (ETM), JHEP **04**, 049 (2010), [arXiv:0909.3187].

[58] A. Bussone *et al.* (ETM), Phys. Rev. D **93**, 11, 114505 (2016), [arXiv:1603.04306].

[59] S. Borsanyi *et al.*, Science **347**, 1452 (2015), [arXiv:1406.4088].

[60] S. Aoki *et al.* (Flavour Lattice Averaging Group), Eur. Phys. J. C **80**, 2, 113 (2020), [arXiv:1902.08191].

[61] M. Hayakawa and S. Uno, Prog. Theor. Phys. **120**, 413 (2008), [arXiv:0804.2044].

[62] N. Carrasco *et al.*, Phys. Rev. **D91**, 7, 074506 (2015), [arXiv:1502.00257].

[63] M. Di Carlo *et al.*, Phys. Rev. D **105**, 7, 074509 (2022), [arXiv:2109.05002].

[64] N. H. Christ *et al.*, Phys. Rev. D **108**, 1, 014501 (2023), [arXiv:2304.08026].

[65] B. Lucini *et al.*, JHEP **02**, 076 (2016), [arXiv:1509.01636].

[66] L. Bushnaq *et al.* (RCstar), JHEP **03**, 012 (2023), [arXiv:2209.13183].

[67] R. Horsley *et al.*, J. Phys. G **43**, 10, 10LT02 (2016), [arXiv:1508.06401].

[68] R. Horsley *et al.* (CSSM, QCDSF, UKQCD), J. Phys. G **46**, 115004 (2019), [arXiv:1904.02304].

[69] Z. R. Kordov *et al.* (CSSM/QCDSF/UKQCD), Phys. Rev. D **101**, 3, 034517 (2020), [arXiv:1911.02186].

[70] T. Ishikawa *et al.*, Phys. Rev. Lett. **109**, 072002 (2012), [arXiv:1202.6018].

[71] M. G. Endres *et al.*, Phys. Rev. Lett. **117**, 7, 072002 (2016), [arXiv:1507.08916].

[72] G. M. de Divitiis *et al.* (RM123), Phys. Rev. **D87**, 11, 114505 (2013), [arXiv:1303.4896].

[73] D. Giusti *et al.*, Phys. Rev. **D95**, 11, 114504 (2017), [arXiv:1704.06561].

[74] P. Boyle *et al.*, JHEP **09**, 153 (2017), [arXiv:1706.05293].

[75] S. Basak *et al.* (MILC), Phys. Rev. D **99**, 3, 034503 (2019), [arXiv:1807.05556].

[76] D. Hatton, C. T. H. Davies and G. P. Lepage, Phys. Rev. D **102**, 9, 094514 (2020), [arXiv:2009.07667].

[77] D. Hatton *et al.*, Phys. Rev. D **103**, 11, 114508 (2021), [arXiv:2102.09609].

[78] F. Bloch and A. Nordsieck, Phys. Rev. **52**, 54 (1937).

[79] D. Giusti *et al.*, Phys. Rev. Lett. **120**, 7, 072001 (2018), [arXiv:1711.06537].

[80] M. Di Carlo *et al.*, Phys. Rev. D **100**, 3, 034514 (2019), [arXiv:1904.08731].

[81] P. Boyle *et al.*, JHEP **02**, 242 (2023), [arXiv:2211.12865].

[82] C. T. Sachrajda *et al.*, PoS **LATTICE2019**, 162 (2019), [arXiv:1910.07342]; C.-Y. Seng *et al.*, JHEP **10**, 179 (2020), [arXiv:2009.00459].

[83] R. Sommer, Nucl. Phys. B **411**, 839 (1994), [hep-lat/9310022].

[84] M. Lüscher, JHEP **08**, 071 (2010), [Erratum: JHEP 03, 092 (2014)], [arXiv:1006.4518].

[85] Y. Aoki *et al.* (Flavour Lattice Averaging Group (FLAG)) (2024), [arXiv:2411.04268].

[86] M. Bruno *et al.* (ALPHA), Phys. Rev. Lett. **114**, 10, 102001 (2015), [arXiv:1410.8374].

[87] A. Bazavov *et al.* (Fermilab Lattice, MILC), Phys. Rev. **D93**, 11, 113016 (2016), [arXiv:1602.03560].

[88] R. J. Dowdall *et al.*, Phys. Rev. **D86**, 094510 (2012), [arXiv:1207.5149].

[89] C. McNeile *et al.*, Phys. Rev. **D86**, 074503 (2012), [arXiv:1207.0994].

[90] S. Schaefer, R. Sommer and F. Virotta (ALPHA), Nucl. Phys. **B845**, 93 (2011), [arXiv:1009.5228].

[91] M. Lüscher, PoS **LATTICE2010**, 015 (2010), [arXiv:1009.5877].

[92] R. Brower *et al.*, Phys. Lett. **B560**, 64 (2003), [hep-lat/0302005].

[93] S. Aoki *et al.*, Phys. Rev. **D76**, 054508 (2007), [arXiv:0707.0396].

[94] C. Bernard and D. Toussaint (MILC), Phys. Rev. D **97**, 7, 074502 (2018), [arXiv:1707.05430].

[95] M. Luscher and S. Schaefer, JHEP **07**, 036 (2011), [arXiv:1105.4749].

[96] N. Husung, P. Marquard and R. Sommer, Eur. Phys. J. C **80**, 3, 200 (2020), [arXiv:1912.08498].

[97] N. Husung, P. Marquard and R. Sommer, Phys. Lett. B **829**, 137069 (2022), [arXiv:2111.02347].

[98] N. Husung, Eur. Phys. J. C **83**, 2, 142 (2023), [arXiv:2206.03536].

[99] G. Colangelo, S. Dürr and C. Haefeli, Nucl. Phys. **B721**, 136 (2005), [hep-lat/0503014].

[100] M. Lüscher, Commun. Math. Phys. **104**, 177 (1986).

[101] G. Martinelli *et al.*, Nucl. Phys. **B445**, 81 (1995), [hep-lat/9411010].

[102] M. Lüscher *et al.*, Nucl. Phys. **B384**, 168 (1992), [hep-lat/9207009].

[103] G. Martinelli *et al.*, Phys. Lett. **B411**, 141 (1997), [hep-lat/9705018].

[104] B. Colquhoun *et al.*, Phys. Rev. **D91**, 7, 074514 (2015), [arXiv:1408.5768].

[105] D. Hatton *et al.* (HPQCD), Phys. Rev. D **100**, 11, 114513 (2019), [arXiv:1909.00756].

[106] M. Lüscher *et al.*, Nucl. Phys. **B413**, 481 (1994), [hep-lat/9309005]; M. Della Morte *et al.* (ALPHA), Nucl. Phys. **B713**, 378 (2005), [hep-lat/0411025].

[107] M. Tomii *et al.* (JLQCD), Phys. Rev. **D94**, 5, 054504 (2016), [arXiv:1604.08702].

[108] F. Karsch, H. Simma and T. Yoshie, PoS **LATTICE2022**, 244 (2023), [arXiv:2212.08392].

[109] S. Duane *et al.*, Phys. Lett. **B195**, 216 (1987).

[110] D. J. E. Callaway and A. Rahman, Phys. Rev. Lett. **49**, 613 (1982).

[111] D. J. E. Callaway and A. Rahman, Phys. Rev. D **28**, 1506 (1983).

[112] J. Polonyi and H. W. Wyld, Phys. Rev. Lett. **51**, 2257 (1983), [Erratum: Phys.Rev.Lett. 52, 401 (1984)].

[113] N. Metropolis *et al.*, J. Chem. Phys. **21**, 1087 (1953).

[114] M. A. Clark and A. D. Kennedy, Phys. Rev. Lett. **98**, 051601 (2007), [hep-lat/0608015].

[115] J. C. Sexton and D. H. Weingarten, Nucl. Phys. B **380**, 665 (1992).

[116] M. Hasenbusch, Phys. Lett. **B519**, 177 (2001), [hep-lat/0107019].

[117] M. Lüscher, JHEP **05**, 052 (2003), [hep-lat/0304007].

[118] M. Lüscher, Comput. Phys. Commun. **156**, 209 (2004), [hep-lat/0310048].

[119] M. Lüscher, JHEP **07**, 081 (2007), [arXiv:0706.2298].

[120] M. Lüscher, JHEP **12**, 011 (2007), [arXiv:0710.5417].

[121] A. Stathopoulos and K. Orginos, SIAM J. Sci. Comput. **32**, 439 (2010), [arXiv:0707.0131].

[122] P. A. Boyle (2014), [arXiv:1402.2585].

[123] R. Babich *et al.*, Phys. Rev. Lett. **105**, 201602 (2010), [arXiv:1005.3043].

[124] A. Frommer *et al.*, SIAM J. Sci. Comput. **36**, A1581 (2014), [arXiv:1303.1377].

[125] M. Bruno, S. Schaefer and R. Sommer (ALPHA), JHEP **08**, 150 (2014), [arXiv:1406.5363].

[126] M. Creutz, Phys. Rev. **D38**, 1228 (1988); R. Gupta, G. W. Kilcup and S. R. Sharpe, Phys. Rev. **D38**, 1278 (1988).

[127] P. Fritzsch *et al.*, PoS **LATTICE2021**, 465 (2022), [arXiv:2111.11544].

[128] M. Cè *et al.*, PoS **LATTICE2021**, 383 (2022), [arXiv:2110.15375].

[129] M. Lüscher, EPJ Web Conf. **175**, 01002 (2018), [arXiv:1707.09758].

[130] G. Parisi, Phys. Rept. **103**, 203 (1984).

[131] G. P. Lepage, in "Theoretical Advanced Study Institute in Elementary Particle Physics," (1989).

[132] E. Shintani *et al.*, Phys. Rev. D **91**, 11, 114511 (2015), [arXiv:1402.0244].

[133] M. Luscher and P. Weisz, JHEP **09**, 010 (2001), [hep-lat/0108014]; H. B. Meyer, JHEP **01**, 048 (2003), [hep-lat/0209145]; H. B. Meyer, JHEP **01**, 030 (2004), [hep-lat/0312034]; M. Cè, L. Giusti and S. Schaefer, Phys. Rev. D **93**, 9, 094507 (2016), [arXiv:1601.04587]; M. Dalla Brida *et al.*, Phys. Lett. B **816**, 136191 (2021), [arXiv:2007.02973]; L. Barca *et al.*, Phys. Rev. D **110**, 5, 054515 (2024), [arXiv:2406.12656].

[134] M. Lüscher and U. Wolff, Nucl. Phys. **B339**, 222 (1990).

[135] J. J. Dudek *et al.*, Phys. Rev. **D82**, 034508 (2010), [arXiv:1004.4930]; J. J. Dudek *et al.*, Phys. Rev. **D83**, 111502 (2011), [arXiv:1102.4299]; R. G. Edwards *et al.*, Phys. Rev. **D84**, 074508 (2011), [arXiv:1104.5152].

[136] G. P. Engel *et al.* (BGR [Bern-Graz-Regensburg]), Phys. Rev. **D82**, 034505 (2010), [arXiv:1005.1748]; D. Mohler *et al.*, Phys. Rev. Lett. **111**, 22, 222001 (2013), [arXiv:1308.3175].

[137] M. S. Mahbub *et al.*, Annals Phys. **342**, 270 (2014), [arXiv:1310.6803].

[138] J. Bulava *et al.*, Nucl. Phys. **B910**, 842 (2016), [arXiv:1604.05593].

[139] R. Brett *et al.*, Nucl. Phys. **B932**, 29 (2018), [arXiv:1802.03100].

[140] B. Hörz and A. Hanlon, Phys. Rev. Lett. **123**, 14, 142002 (2019), [arXiv:1905.04277].

[141] J. E. Mandula, G. Zweig and J. Govaerts, Nucl. Phys. **B228**, 91 (1983); J. E. Mandula and E. Shpiz, Nucl. Phys. **B232**, 180 (1984).

[142] H. B. Meyer and M. J. Teper, Nucl. Phys. **B658**, 113 (2003), [hep-lat/0212026].

[143] O. Bar, A. Broll and R. Sommer, Eur. Phys. J. C **83**, 8, 757 (2023), [arXiv:2306.02703].

[144] P. F. Bedaque, Phys. Lett. B **593**, 82 (2004), [arXiv:nucl-th/0402051].

[145] P. F. Bedaque and J.-W. Chen, Phys. Lett. B **616**, 208 (2005), [hep-lat/0412023].

[146] G. M. de Divitiis, R. Petronzio and N. Tantalo, Phys. Lett. B **595**, 408 (2004), [hep-lat/0405002].

[147] C. Bourrely, B. Machet and E. de Rafael, Nucl. Phys. **B189**, 157 (1981).

[148] C. G. Boyd, B. Grinstein and R. F. Lebed, Phys. Rev. Lett. **74**, 4603 (1995), [hep-ph/9412324].

[149] T. Becher and R. J. Hill, Phys. Lett. **B633**, 61 (2006), [hep-ph/0509090].

[150] C. Bourrely, I. Caprini and L. Lellouch, Phys. Rev. **D79**, 013008 (2009), [Erratum: Phys. Rev. D82, 099902(2010)], [arXiv:0807.2722].

[151] M. Lüscher, Commun. Math. Phys. **105**, 153 (1986); M. Lüscher, Nucl. Phys. **B364**, 237 (1991).

[152] L. Maiani and M. Testa, Phys. Lett. **B245**, 585 (1990).

[153] M. T. Hansen, H. B. Meyer and D. Robaina, Phys. Rev. **D96**, 9, 094513 (2017), [arXiv:1704.08993].

[154] M. Hansen, A. Lupo and N. Tantalo, Phys. Rev. **D99**, 9, 094508 (2019), [arXiv:1903.06476]; J. Bulava and M. T. Hansen, Phys. Rev. D **100**, 3, 034521 (2019), [arXiv:1903.11735]; M. Bruno and M. T. Hansen, JHEP **06**, 043 (2021), [arXiv:2012.11488].

[155] J. Bulava *et al.*, JHEP **07**, 034 (2022), [arXiv:2111.12774]; T. Bergamaschi, W. I. Jay and P. R. Oare, Phys. Rev. D **108**, 7, 074516 (2023), [arXiv:2305.16190]; L. Del Debbio *et al.*, Eur. Phys. J. C **85**, 2, 185 (2025), [arXiv:2409.04413]; A. Patella and N. Tantalo, JHEP **01**, 091 (2025), [arXiv:2407.02069]; M. Bruno, L. Giusti and M. Saccardi, Phys. Rev. D **111**, 9, 094515 (2025), [arXiv:2407.04141].

[156] A. Evangelista *et al.* (Extended Twisted Mass), Phys. Rev. D **108**, 7, 074513 (2023), [arXiv:2308.03125].

[157] V. Bernard *et al.*, JHEP **01**, 019 (2011), [arXiv:1010.6018]; M. Doring *et al.*, Eur. Phys. J. **A47**, 139 (2011), [arXiv:1107.3988]; R. A. Briceño and Z. Davoudi, Phys. Rev. **D88**, 9, 094507 (2013), [arXiv:1204.1110]; M. T. Hansen and S. R. Sharpe, Phys. Rev. **D86**, 016007 (2012), [arXiv:1204.0826].

[158] R. A. Briceno, Phys. Rev. D **89**, 7, 074507 (2014), [arXiv:1401.3312].

[159] N. Ishii, S. Aoki and T. Hatsuda, Phys. Rev. Lett. **99**, 022001 (2007), [arXiv:nucl-th/0611096]; N. Ishii *et al.* (HAL QCD), Phys. Lett. B **712**, 437 (2012), [arXiv:1203.3642].

[160] M. Fischer *et al.* (Extended Twisted Mass, ETM), Phys. Lett. B **819**, 136449 (2021), [arXiv:2006.13805]; Y. Lyu *et al.*, Phys. Rev. Lett. **131**, 16, 161901 (2023), [arXiv:2302.04505]; P. Boyle *et al.*, Phys. Rev. Lett. **134**, 11, 111901 (2025), [arXiv:2406.19194]; Z. Wang *et al.* (2025), [arXiv:2502.03700].

[161] S. M. Dawid *et al.* (2025), [arXiv:2502.14348]; S. M. Dawid *et al.* (2025), [arXiv:2502.17976].

[162] F. Romero-López, PoS **LATTICE2022**, 235 (2023), [arXiv:2212.13793]; L. Liu, PoS **LATTICE2022**, 234 (2023); A. D. Hanlon, PoS **LATTICE2023**, 106 (2024), [arXiv:2402.05185]; J. T. Tsang, in "41st International Symposium on Lattice Field Theory," (2025), [arXiv:2503.05554].

[163] T. Inoue *et al.* (HAL QCD), Phys. Rev. **C91**, 1, 011001 (2015), [arXiv:1408.4892]; J. R. Green *et al.*, Phys. Rev. Lett. **127**, 24, 242003 (2021), [arXiv:2103.01054]; W. Detmold *et al.* (NPLQCD), Phys. Rev. D **111**, 11, 114501 (2025), [arXiv:2404.12039]; J. Bulava *et al.* (BaSc) (2025), [arXiv:2505.05547].

[164] J. R. Green, in "11th International Workshop on Chiral Dynamics," (2025), [arXiv:2502.15546]; C. Morningstar, in "11th International Workshop on Chiral Dynamics," (2025), [arXiv:2504.01950].

[165] K. Polejaeva and A. Rusetsky, Eur. Phys. J. **A48**, 67 (2012), [arXiv:1203.1241]; R. A. Briceno and Z. Davoudi, Phys. Rev. **D87**, 9, 094507 (2013), [arXiv:1212.3398]; M. T. Hansen and S. R. Sharpe, Phys. Rev. **D90**, 11, 116003 (2014), [arXiv:1408.5933]; M. T. Hansen and S. R. Sharpe, Phys. Rev. **D92**, 11, 114509 (2015), [arXiv:1504.04248]; R. Briceño, M. T. Hansen and S. R. Sharpe, Phys. Rev. **D95**, 7, 074510 (2017), [arXiv:1701.07465]; H. W. Hammer, J. Y. Pang and A. Rusetsky, JHEP **10**, 115 (2017), [arXiv:1707.02176]; R. A. Briceno, M. T. Hansen and S. R. Sharpe, Phys. Rev. **D99**, 1, 014516 (2019), [arXiv:1810.01429]; M. Mai and M. Döring, Eur. Phys. J. **A53**, 12, 240 (2017), [arXiv:1709.08222]; M. T. Hansen, F. Romero-López and S. R. Sharpe, JHEP **07**, 047 (2020), [Erratum: JHEP 02, 014 (2021)], [arXiv:2003.10974]; T. D. Blanton and S. R. Sharpe, Phys. Rev. D **103**, 5, 054503 (2021), [arXiv:2011.05520]; T. D. Blanton and S. R. Sharpe, Phys. Rev. D **104**, 3, 034509 (2021), [arXiv:2105.12094]; Z. T. Draper *et al.*, JHEP **07**, 226 (2023), [arXiv:2303.10219]; Z. T. Draper and S. R. Sharpe, JHEP **07**, 083 (2024), [arXiv:2403.20064].

[166] T. D. Blanton, F. Romero-López and S. R. Sharpe, Phys. Rev. Lett. **124**, 3, 032001 (2020), [arXiv:1909.02973]; C. Culver *et al.*, Phys. Rev. D **101**, 11, 114507 (2020), [arXiv:1911.09047]; A. Alexandru *et al.*, Phys. Rev. D **102**, 11, 114523 (2020), [arXiv:2009.12358]; R. Brett *et al.*, Phys. Rev. D **104**, 1, 014501 (2021), [arXiv:2101.06144]; Z. T. Draper *et al.*, JHEP **05**, 137 (2023), [arXiv:2302.13587].

[167] M. Mai *et al.* (GWQCD), Phys. Rev. Lett. **127**, 22, 222001 (2021), [arXiv:2107.03973]; H. Yan *et al.*, Phys. Rev. Lett. **133**, 21, 211906 (2024), [arXiv:2407.16659].

[168] M. T. Hansen, F. Romero-López and S. R. Sharpe, JHEP **06**, 051 (2024), [arXiv:2401.06609]; S. M. Dawid, F. Romero-López and S. R. Sharpe, JHEP **01**, 060 (2025), [arXiv:2409.17059].

[169] M. T. Hansen and S. R. Sharpe, Ann. Rev. Nucl. Part. Sci. **69**, 65 (2019), [arXiv:1901.00483]; M. Mai, M. Döring and A. Rusetsky, Eur. Phys. J. ST **230**, 6, 1623 (2021), [arXiv:2103.00577]; F. Romero-López, in "11th International Workshop on Chiral Dynamics," (2025), [arXiv:2504.00586].

[170] L. Lellouch and M. Lüscher, Commun. Math. Phys. **219**, 31 (2001), [hep-lat/0003023].

[171] T. Blum *et al.*, Phys. Rev. Lett. **108**, 141601 (2012), [arXiv:1111.1699]; T. Blum *et al.*, Phys. Rev. **D86**, 074513 (2012), [arXiv:1206.5142].

[172] T. Blum *et al.*, Phys. Rev. **D91**, 7, 074502 (2015), [arXiv:1502.00263].

[173] R. Briceño, M. T. Hansen and A. Walker-Loud, Phys. Rev. **D91**, 3, 034501 (2015), [arXiv:1406.5965].

[174] R. Briceño and M. T. Hansen, Phys. Rev. **D94**, 1, 013008 (2016), [arXiv:1509.08507].

[175] R. Briceño *et al.*, Phys. Rev. **D93**, 11, 114508 (2016), [arXiv:1604.03530].

[176] C. Alexandrou *et al.*, Phys. Rev. D **98**, 7, 074502 (2018), [Erratum: Phys.Rev.D 105, 019902 (2022)], [arXiv:1807.08357].

[177] A. Radhakrishnan, J. J. Dudek and R. G. Edwards (Hadron Spectrum), Phys. Rev. D **106**, 11, 114513 (2022), [arXiv:2208.13755].

[178] L. Leskovec *et al.*, Phys. Rev. Lett. **134**, 16, 161901 (2025), [arXiv:2501.00903].

[179] F. Müller and A. Rusetsky, JHEP **03**, 152 (2021), [arXiv:2012.13957].

[180] M. T. Hansen, F. Romero-López and S. R. Sharpe, JHEP **04**, 113 (2021), [arXiv:2101.10246].

[181] D. Agadjanov *et al.*, JHEP **06**, 043 (2016), [arXiv:1603.07205].

[182] S. Hashimoto, PTEP **2017**, 5, 053B03 (2017), [arXiv:1703.01881].

[183] G. Bailas, S. Hashimoto and T. Ishikawa, PTEP **2020**, 4, 043B07 (2020), [arXiv:2001.11779].

[184] C. Alexandrou *et al.* (Extended Twisted Mass Collaboration (ETMC)), Phys. Rev. Lett. **130**, 24, 241901 (2023), [arXiv:2212.08467].

[185] C. Alexandrou *et al.* (Extended Twisted Mass), Phys. Rev. Lett. **132**, 26, 261901 (2024), [arXiv:2403.05404].

[186] P. Gambino and S. Hashimoto, Phys. Rev. Lett. **125**, 3, 032001 (2020), [arXiv:2005.13730].

[187] P. Gambino *et al.*, JHEP **07**, 083 (2022), [arXiv:2203.11762].

[188] A. Barone *et al.*, JHEP **07**, 145 (2023), [arXiv:2305.14092].

[189] R. Kellermann *et al.* (2025), [arXiv:2504.03358].

[190] A. De Santis *et al.* (2025), [arXiv:2504.06063].

[191] H. Fukaya *et al.*, Phys. Rev. D **102**, 11, 114516 (2020), [arXiv:2010.01253].

[192] G. Colangelo *et al.*, Eur. Phys. J. C **71**, 1695 (2011), [arXiv:1011.4408].

[193] S. Aoki *et al.*, Eur. Phys. J. C **74**, 2890 (2014), [arXiv:1310.8555].

[194] S. Aoki *et al.*, Eur. Phys. J. **C77**, 2, 112 (2017), [arXiv:1607.00299].

[195] Y. Aoki *et al.* (Flavour Lattice Averaging Group (FLAG)), Eur. Phys. J. C **82**, 10, 869 (2022), [arXiv:2111.09849].

[196] C. Bernard *et al.*, Nucl. Phys. Proc. Suppl. **119**, 170 (2003), [hep-lat/0209086].

[197] Y. Aoki *et al.*, PoS **LATTICE2024**, 412 (2025), [arXiv:2502.08303].

[198] S. Perantonis and C. Michael, Nucl. Phys. **B347**, 854 (1990).

[199] G. S. Bali and K. Schilling, Phys. Rev. **D46**, 2636 (1992).

[200] S. Necco and R. Sommer, Nucl. Phys. **B622**, 328 (2002), [hep-lat/0108008].

[201] J. M. Blairon *et al.*, Nucl. Phys. **B180**, 439 (1981).

[202] H. Fukaya *et al.* (JLQCD), Phys. Rev. Lett. **104**, 122002 (2010), [Erratum: Phys. Rev. Lett.105,159901(2010)], [arXiv:0911.5555].

[203] H. Fukaya *et al.* (JLQCD, TWQCD), Phys. Rev. **D83**, 074501 (2011), [arXiv:1012.4052].

[204] L. Giusti and M. Lüscher, JHEP **03**, 013 (2009), [arXiv:0812.3638].

[205] K. Cichy, E. Garcia-Ramos and K. Jansen, JHEP **10**, 175 (2013), [arXiv:1303.1954].

[206] G. P. Engel *et al.*, Phys. Rev. Lett. **114**, 11, 112001 (2015), [arXiv:1406.4987].

[207] G. P. Engel *et al.*, Phys. Rev. **D91**, 5, 054505 (2015), [arXiv:1411.6386].

[208] G. Cossu *et al.*, PTEP **2016**, 9, 093B06 (2016), [arXiv:1607.01099].

[209] G. S. Bali *et al.* (RQCD), JHEP **08**, 137 (2021), [arXiv:2106.05398].

[210] T. Blum *et al.* (RBC, UKQCD), Phys. Rev. **D93**, 7, 074505 (2016), [arXiv:1411.7017].
[211] P. A. Boyle *et al.* (RBC, UKQCD), Phys. Rev. D **110**, 3, 034501 (2024), [arXiv:2404.02297].
[212] B. J. Choi *et al.* (SWME), Phys. Rev. **D93**, 1, 014511 (2016), [arXiv:1509.00592].
[213] J. Laiho and R. S. Van de Water, PoS **LATTICE2011**, 293 (2011), [arXiv:1112.4861].
[214] T. Blum *et al.* (RBC, UKQCD), Phys. Rev. D **93**, 7, 074505 (2016), [arXiv:1411.7017].
[215] B. J. Choi *et al.* (SWME), Phys. Rev. D **93**, 1, 014511 (2016), [arXiv:1509.00592].
[216] E. Gamiz *et al.* (HPQCD), Phys. Rev. **D80**, 014503 (2009), [arXiv:0902.1815].
[217] R. J. Dowdall *et al.*, Phys. Rev. D **100**, 9, 094508 (2019), [arXiv:1907.01025].
[218] Y. Aoki *et al.*, Phys. Rev. **D91**, 11, 114505 (2015), [arXiv:1406.6192].
[219] N. Carrasco *et al.* (ETM), Phys. Rev. D **92**, 3, 034516 (2015), [arXiv:1505.06639].
[220] A. Bazavov *et al.*, Phys. Rev. **D97**, 3, 034513 (2018), [arXiv:1706.04622].
[221] M. Ademollo and R. Gatto, Phys. Rev. Lett. **13**, 264 (1964).
[222] H. Leutwyler and M. Roos, Z. Phys. **C25**, 91 (1984).
[223] P. A. Boyle *et al.*, Phys. Rev. Lett. **100**, 141601 (2008), [arXiv:0710.5136].
[224] V. Lubicz *et al.* (ETM), Phys. Rev. **D80**, 111502 (2009), [arXiv:0906.4728]; V. Lubicz *et al.* (ETM), PoS **LATTICE2010**, 316 (2010), [arXiv:1012.3573].
[225] P. A. Boyle *et al.* (RBC-UKQCD), Eur. Phys. J. **C69**, 159 (2010), [arXiv:1004.0886].
[226] A. Bazavov *et al.*, Phys. Rev. **D87**, 073012 (2013), [arXiv:1212.4993].
[227] T. Kaneko *et al.* (JLQCD), PoS **LATTICE2012**, 111 (2012), [arXiv:1211.6180].
[228] P. A. Boyle *et al.*, JHEP **08**, 132 (2013), [arXiv:1305.7217].
[229] P. A. Boyle *et al.* (RBC/UKQCD), JHEP **06**, 164 (2015), [arXiv:1504.01692].
[230] N. Carrasco *et al.*, Phys. Rev. **D93**, 11, 114512 (2016), [arXiv:1602.04113].
[231] A. Bazavov *et al.* (Fermilab Lattice, MILC), Phys. Rev. D **99**, 11, 114509 (2019), [arXiv:1809.02827].
[232] K.-i. Ishikawa *et al.* (PACS), Phys. Rev. D **106**, 9, 094501 (2022), [arXiv:2206.08654].
[233] H. Na *et al.*, Phys. Rev. **D82**, 114506 (2010), [arXiv:1008.4562].
[234] H. Na *et al.*, Phys. Rev. **D84**, 114505 (2011), [arXiv:1109.1501].
[235] V. Lubicz *et al.* (ETM), Phys. Rev. **D96**, 5, 054514 (2017), [Erratum: Phys. Rev. D99, 099902(2019)], [arXiv:1706.03017].
[236] T. Kaneko *et al.* (JLQCD), EPJ Web Conf. **175**, 13007 (2018), [arXiv:1711.11235].
[237] B. Chakraborty *et al.* ((HPQCD Collaboration)§, HPQCD), Phys. Rev. D **104**, 3, 034505 (2021), [arXiv:2104.09883].
[238] A. Bazavov *et al.* (Fermilab Lattice, MILC), Phys. Rev. D **107**, 9, 094516 (2023), [arXiv:2212.12648].
[239] S. Meinel, Phys. Rev. Lett. **118**, 8, 082001 (2017), [arXiv:1611.09696].
[240] S. Meinel, Phys. Rev. D **97**, 3, 034511 (2018), [arXiv:1712.05783].
[241] E. Dalgic *et al.*, Phys. Rev. **D73**, 074502 (2006), [Erratum: Phys. Rev. D75,119906(2007)], [hep-lat/0601021].
[242] J. M. Flynn *et al.*, Phys. Rev. **D91**, 7, 074510 (2015), [arXiv:1501.05373].
[243] J. A. Bailey *et al.* (Fermilab Lattice, MILC), Phys. Rev. **D92**, 1, 014024 (2015), [arXiv:1503.07839].

[244] B. Colquhoun *et al.*, Phys. Rev. **D93**, 3, 034502 (2016), [arXiv:1510.07446].

[245] Z. Gelzer *et al.*, EPJ Web Conf. **175**, 13024 (2018), [arXiv:1710.09442].

[246] B. Colquhoun *et al.* (JLQCD), Phys. Rev. D **106**, 5, 054502 (2022), [arXiv:2203.04938].

[247] C. M. Bouchard *et al.*, Phys. Rev. D **90**, 054506 (2014), [arXiv:1406.2279].

[248] C. J. Monahan *et al.*, Phys. Rev. D **98**, 11, 114509 (2018), [arXiv:1808.09285].

[249] A. Bazavov *et al.* (Fermilab Lattice, MILC), Phys. Rev. D **100**, 3, 034501 (2019), [arXiv:1901.02561].

[250] J. M. Flynn *et al.* (RBC/UKQCD), Phys. Rev. D **107**, 11, 114512 (2023), [arXiv:2303.11280].

[251] M. C. Arnesen *et al.*, Phys. Rev. Lett. **95**, 071802 (2005), [hep-ph/0504209]; J. A. Bailey *et al.*, Phys. Rev. **D79**, 054507 (2009), [arXiv:0811.3640].

[252] L. Lellouch, Nucl. Phys. B **479**, 353 (1996), [hep-ph/9509358].

[253] M. Di Carlo *et al.*, Phys. Rev. D **104**, 5, 054502 (2021), [arXiv:2105.02497].

[254] G. Martinelli, S. Simula and L. Vittorio, JHEP **08**, 022 (2022), [arXiv:2202.10285].

[255] J. M. Flynn, A. Jüttner and J. T. Tsang (2023), [arXiv:2303.11285].

[256] T. Blake *et al.*, Phys. Rev. D **108**, 9, 094509 (2023), [arXiv:2205.06041].

[257] J. Harrison, Phys. Rev. D **110**, 5, 054506 (2024), [arXiv:2405.01390].

[258] A. Gopal and N. Gubernari, Phys. Rev. D **111**, 3, L031501 (2025), [arXiv:2412.04388].

[259] S. Hashimoto *et al.*, Phys. Rev. **D61**, 014502 (1999), [hep-ph/9906376]; S. Hashimoto *et al.*, Phys. Rev. **D66**, 014503 (2002), [hep-ph/0110253].

[260] C. Bernard *et al.*, Phys. Rev. **D79**, 014506 (2009), [arXiv:0808.2519]; J. A. Bailey *et al.* (Fermilab Lattice, MILC), Phys. Rev. **D89**, 11, 114504 (2014), [arXiv:1403.0635]; J. Harrison, C. Davies and M. Wingate (HPQCD), Phys. Rev. **D97**, 5, 054502 (2018), [arXiv:1711.11013]; E. McLean *et al.*, Phys. Rev. **D99**, 11, 114512 (2019), [arXiv:1904.02046]; T. Bhattacharya *et al.* (LANL/SWME), PoS **LATTICE2018**, 283 (2018).

[261] J. A. Bailey *et al.* (MILC), Phys. Rev. **D92**, 3, 034506 (2015), [arXiv:1503.07237].

[262] H. Na *et al.* (HPQCD), Phys. Rev. **D92**, 5, 054510 (2015), [Erratum: Phys. Rev. D93, 19906(2016)], [arXiv:1505.03925].

[263] E. McLean *et al.*, Phys. Rev. D **101**, 7, 074513 (2020), [arXiv:1906.00701].

[264] A. Bazavov *et al.* (Fermilab Lattice, MILC, Fermilab Lattice, MILC), Eur. Phys. J. C **82**, 12, 1141 (2022), [Erratum: Eur.Phys.J.C 83, 21 (2023)], [arXiv:2105.14019].

[265] J. Harrison and C. T. H. Davies (HPQCD, (HPQCD Collaboration)‡), Phys. Rev. D **109**, 9, 094515 (2024), [arXiv:2304.03137].

[266] Y. Aoki *et al.* (JLQCD), Phys. Rev. D **109**, 7, 074503 (2024), [arXiv:2306.05657].

[267] W. Detmold, C. Lehner and S. Meinel, Phys. Rev. **D92**, 3, 034503 (2015), [arXiv:1503.01421].

[268] N. H. Christ *et al.* (RBC, UKQCD), Phys. Rev. **D92**, 9, 094512 (2015), [arXiv:1507.03094]; N. H. Christ *et al.* (RBC, UKQCD), Phys. Rev. **D93**, 11, 114517 (2016), [arXiv:1605.04442]; N. H. Christ *et al.*, Phys. Rev. **D94**, 11, 114516 (2016), [arXiv:1608.07585]; Z. Bai *et al.*, Phys. Rev. Lett. **118**, 25, 252001 (2017), [arXiv:1701.02858]; Z. Bai *et al.*, Phys. Rev. **D98**, 7, 074509 (2018), [arXiv:1806.11520]; N. H. Christ *et al.* (RBC, UKQCD), Phys. Rev. D **100**, 11, 114506 (2019), [arXiv:1910.10644].

[269] P. A. Boyle *et al.* (RBC, UKQCD), Phys. Rev. D **107**, 1, L011503 (2023), [arXiv:2202.08795].

[270] F. Erben *et al.* (2025), [arXiv:2504.07727].

[271] R. Frezzotti *et al.* (2025), [arXiv:2508.03655].

[272] R. R. Horgan *et al.*, Phys. Rev. **D89**, 9, 094501 (2014), [arXiv:1310.3722]; J. A. Bailey *et al.*, Phys. Rev. **D93**, 2, 025026 (2016), [arXiv:1509.06235]; D. Du *et al.*, Phys. Rev. **D93**, 3, 034005 (2016), [arXiv:1510.02349].

[273] W. G. Parrott, C. Bouchard and C. T. H. Davies ((HPQCD collaboration)§, HPQCD), Phys. Rev. D **107**, 1, 014510 (2023), [arXiv:2207.12468].

[274] W. Detmold and S. Meinel, Phys. Rev. **D93**, 7, 074501 (2016), [arXiv:1602.01399].

[275] Z. Bai *et al.*, Phys. Rev. Lett. **113**, 112003 (2014), [arXiv:1406.0916].

[276] N. H. Christ *et al.*, Phys. Rev. D **91**, 11, 114510 (2015), [arXiv:1504.01170].

[277] Z. Bai *et al.*, Phys. Rev. D **109**, 5, 054501 (2024), [arXiv:2309.01193].

[278] N. Christ *et al.*, Phys. Rev. Lett. **130**, 19, 191901 (2023), [arXiv:2208.03834].

[279] E.-H. Chao and N. Christ, Phys. Rev. D **110**, 5, 054514 (2024), [arXiv:2406.07447].

[280] A. Desiderio *et al.*, Phys. Rev. D **103**, 1, 014502 (2021), [arXiv:2006.05358]; G. Gagliardi *et al.*, Phys. Rev. D **105**, 11, 114507 (2022), [arXiv:2202.03833]; D. Giusti *et al.*, Phys. Rev. D **107**, 7, 074507 (2023), [arXiv:2302.01298]; R. Frezzotti *et al.*, Phys. Rev. D **108**, 7, 074505 (2023), [arXiv:2306.05904]; R. Frezzotti *et al.*, Phys. Rev. D **109**, 11, 114506 (2024), [arXiv:2402.03262]; R. Di Palma *et al.*, Phys. Rev. D **111**, 11, 114523 (2025), [arXiv:2504.08680]; D. Giusti *et al.* (2025), [arXiv:2505.11757].

[281] P.-X. Ma *et al.*, Phys. Rev. D **103**, 114503 (2021), [arXiv:2102.12048]; J.-S. Yoo *et al.*, Phys. Rev. D **108**, 3, 034508 (2023), [arXiv:2305.03198].

[282] P.-X. Ma *et al.* (2023), [arXiv:2308.16755].

[283] G. P. Lepage and P. B. Mackenzie, Phys. Rev. D **48**, 2250 (1993), [hep-lat/9209022].

[284] C. T. H. Davies *et al.* (HPQCD), Phys. Rev. **D78**, 114507 (2008), [arXiv:0807.1687].

[285] C. McNeile *et al.*, Phys. Rev. **D82**, 034512 (2010), [arXiv:1004.4285].

[286] A. Bochkarev and P. de Forcrand, Nucl. Phys. B **477**, 489 (1996), [hep-lat/9505025].

[287] E. Shintani *et al.*, Phys. Rev. **D82**, 7, 074505 (2010), [Erratum: Phys. Rev. D89, 099903(2014)], [arXiv:1002.0371].

[288] R. J. Hudspith *et al.*, Mod. Phys. Lett. **A31**, 32, 1630037 (2016).

[289] R. J. Hudspith *et al.* (2018), [arXiv:1804.10286].

[290] S. Cali *et al.*, Phys. Rev. Lett. **125**, 242002 (2020), [arXiv:2003.05781].

[291] I. Allison *et al.* (HPQCD), Phys. Rev. **D78**, 054513 (2008), [arXiv:0805.2999].

[292] B. Chakraborty *et al.*, Phys. Rev. **D91**, 5, 054508 (2015), [arXiv:1408.4169].

[293] Y. Maezawa and P. Petreczky, Phys. Rev. **D94**, 3, 034507 (2016), [arXiv:1606.08798].

[294] P. Petreczky and J. H. Weber, Phys. Rev. D **100**, 3, 034519 (2019), [arXiv:1901.06424].

[295] Q. Mason *et al.* (HPQCD, UKQCD), Phys. Rev. Lett. **95**, 052002 (2005), [hep-lat/0503005].

[296] A. Bazavov *et al.*, Phys. Rev. **D86**, 114031 (2012), [arXiv:1205.6155].

[297] A. Bazavov *et al.*, Phys. Rev. **D90**, 7, 074038 (2014), [arXiv:1407.8437].

[298] F. Karbstein, M. Wagner and M. Weber, Phys. Rev. **D98**, 11, 114506 (2018), [arXiv:1804.10909].

[299] H. Takaura *et al.*, JHEP **04**, 155 (2019), [arXiv:1808.01643].

[300] A. Bazavov *et al.* (TUMQCD), Phys. Rev. D **100**, 11, 114511 (2019), [arXiv:1907.11747].

[301] B. Blossier *et al.*, Phys. Rev. **D85**, 034503 (2012), [arXiv:1110.5829]; B. Blossier *et al.*, Phys. Rev. Lett. **108**, 262002 (2012), [arXiv:1201.5770].

[302] S. Zafeiropoulos *et al.*, Phys. Rev. Lett. **122**, 16, 162002 (2019), [arXiv:1902.08148].

[303] S. Aoki *et al.* (PACS-CS), JHEP **10**, 053 (2009), [arXiv:0906.3906].

[304] P. Fritzsch *et al.*, PoS **LATTICE2014**, 291 (2014), [arXiv:1411.7648].

[305] M. Bruno *et al.* (ALPHA), Phys. Rev. Lett. **119**, 10, 102001 (2017), [arXiv:1706.03821].

[306] M. Dalla Brida *et al.* (ALPHA), Phys. Rev. D **95**, 1, 014507 (2017), [arXiv:1607.06423].

[307] M. Dalla Brida *et al.* (ALPHA), Phys. Lett. B **807**, 135571 (2020), [arXiv:1912.06001].

[308] M. Dalla Brida *et al.* (ALPHA), Eur. Phys. J. C **82**, 12, 1092 (2022), [arXiv:2209.14204].

[309] C. Ayala, X. Lobregat and A. Pineda, JHEP **09**, 016 (2020), [arXiv:2005.12301].

[310] K. Maltman *et al.*, Phys. Rev. D **78**, 114504 (2008), [arXiv:0807.2020].

[311] P. Petreczky and J. H. Weber, Eur. Phys. J. C **82**, 1, 64 (2022), [arXiv:2012.06193].

[312] S. Dürr *et al.*, Phys. Lett. **B701**, 265 (2011), [arXiv:1011.2403].

[313] S. Dürr *et al.*, JHEP **08**, 148 (2011), [arXiv:1011.2711].

[314] A. T. Lytle *et al.* (HPQCD), Phys. Rev. D **98**, 1, 014513 (2018), [arXiv:1805.06225].

[315] C. Alexandrou *et al.* (Extended Twisted Mass), Phys. Rev. D **104**, 7, 074515 (2021), [arXiv:2104.13408].

[316] S. Capitani *et al.*, Nucl. Phys. **B544**, 669 (1999), [Erratum: Nucl. Phys. B582, 762(2000)], [hep-lat/9810063].

[317] M. Bruno *et al.* (ALPHA), PoS **LATTICE2018**, 220 (2019), [arXiv:1903.04094].

[318] A. Bussone *et al.* (ETM), Phys. Rev. **D93**, 11, 114505 (2016), [arXiv:1603.04306].

[319] J. Komijani, JHEP **08**, 062 (2017), [arXiv:1701.00347]; N. Brambilla *et al.* (TUMQCD), Phys. Rev. D **97**, 3, 034503 (2018), [arXiv:1712.04983].

[320] A. Bazavov *et al.* (Fermilab Lattice, MILC, TUMQCD), Phys. Rev. D **98**, 5, 054517 (2018), [arXiv:1802.04248].

[321] Z. Fodor *et al.*, Phys. Rev. Lett. **117**, 8, 082001 (2016), [arXiv:1604.07112].

[322] D. P. Aguillard *et al.* (Muon g-2) (2025), [arXiv:2506.03069].

[323] R. Aliberti *et al.* (2025), [arXiv:2505.21476].

[324] T. Blum, M. Hayakawa and T. Izubuchi, PoS **LATTICE2012**, 022 (2012), [arXiv:1301.2607].

[325] C. Davies, PoS **LATTICE2024**, 019 (2025), [arXiv:2503.03364].

[326] T. Blum, Phys. Rev. Lett. **91**, 052001 (2003), [hep-lat/0212018].

[327] D. Bernecker and H. B. Meyer, Eur. Phys. J. A **47**, 148 (2011), [arXiv:1107.4388].

[328] S. Borsanyi *et al.*, Nature **593**, 7857, 51 (2021), [arXiv:2002.12347].

[329] T. Blum *et al.* (RBC, UKQCD), Phys. Rev. Lett. **121**, 2, 022003 (2018), [arXiv:1801.07224].

[330] C. Lehner and A. S. Meyer, Phys. Rev. D **101**, 074515 (2020), [arXiv:2003.04177].

[331] G. Wang *et al.* (chiQCD), Phys. Rev. D **107**, 3, 034513 (2023), [arXiv:2204.01280].

[332] C. Aubin *et al.*, Phys. Rev. D **106**, 5, 054503 (2022), [arXiv:2204.12256].

[333] M. Cè *et al.*, Phys. Rev. D **106**, 11, 114502 (2022), [arXiv:2206.06582].

[334] C. Alexandrou *et al.* (Extended Twisted Mass), Phys. Rev. D **107**, 7, 074506 (2023), [arXiv:2206.15084].

[335] A. Bazavov *et al.* (Fermilab Lattice, HPQCD,, MILC), Phys. Rev. D **107**, 11, 114514 (2023), [arXiv:2301.08274].

[336] T. Blum *et al.* (RBC, UKQCD), Phys. Rev. D **108**, 5, 054507 (2023), [arXiv:2301.08696].

[337] A. Boccaletti *et al.* (2024), [arXiv:2407.10913].

[338] D. Giusti *et al.*, Phys. Rev. D **99**, 11, 114502 (2019), [arXiv:1901.10462].

[339] S. Kuberski *et al.*, JHEP **03**, 172 (2024), [arXiv:2401.11895].

[340] S. Spiegel and C. Lehner, Phys. Rev. D **111**, 11, 114517 (2025), [arXiv:2410.17053].

[341] T. Blum *et al.* (RBC, UKQCD), Phys. Rev. Lett. **134**, 20, 201901 (2025), [arXiv:2410.20590].

[342] D. Djukanovic *et al.*, JHEP **04**, 098 (2025), [arXiv:2411.07969].

[343] C. Alexandrou *et al.* (Extended Twisted Mass), Phys. Rev. D **111**, 5, 054502 (2025), [arXiv:2411.08852].

[344] A. Bazavov *et al.* (MILC, Fermilab Lattice, HPQCD), Phys. Rev. D **111**, 9, 094508 (2025), [arXiv:2411.09656].

[345] A. Bazavov *et al.* (Fermilab Lattice, HPQCD,, MILC), Phys. Rev. Lett. **135**, 1, 011901 (2025), [arXiv:2412.18491].

[346] T. Aoyama *et al.*, Phys. Rept. **887**, 1 (2020), [arXiv:2006.04822].

[347] G. Colangelo *et al.*, Phys. Lett. B **833**, 137313 (2022), [arXiv:2205.12963].

[348] F. V. Ignatov *et al.* (CMD-3), Phys. Rev. Lett. **132**, 23, 231903 (2024), [arXiv:2309.12910].

[349] M. Cè *et al.*, JHEP **08**, 220 (2022), [arXiv:2203.08676].

[350] C. T. H. Davies *et al.*, Phys. Rev. D **111**, 1, 014513 (2025), [arXiv:2410.23832].

[351] T. Blum *et al.*, Phys. Rev. Lett. **124**, 13, 132002 (2020), [arXiv:1911.08123].

[352] E.-H. Chao *et al.*, Eur. Phys. J. C **81**, 7, 651 (2021), [arXiv:2104.02632].

[353] E.-H. Chao *et al.*, Eur. Phys. J. C **82**, 8, 664 (2022), [arXiv:2204.08844].

[354] T. Blum *et al.* (2023), [arXiv:2304.04423].

[355] Z. Fodor *et al.*, Phys. Rev. D **111**, 11, 114509 (2025), [arXiv:2411.11719].

[356] A. Gérardin, H. B. Meyer and A. Nyffeler, Phys. Rev. D **100**, 3, 034520 (2019), [arXiv:1903.09471].

[357] A. Gérardin *et al.*, Phys. Rev. D **111**, 5, 054511 (2025), [arXiv:2305.04570].

[358] C. Alexandrou *et al.* (Extended Twisted Mass), Phys. Rev. D **108**, 9, 094514 (2023), [arXiv:2308.12458].

[359] T. Lin *et al.*, Rept. Prog. Phys. **88**, 8, 080501 (2025), [arXiv:2411.06349].

[360] O. Bar, Phys. Rev. D **99**, 5, 054506 (2019), [arXiv:1812.09191].

[361] C. C. Chang *et al.*, Nature **558**, 7708, 91 (2018), [arXiv:1805.12130].

[362] D. Djukanovic *et al.*, Phys. Rev. Lett. **132**, 21, 211901 (2024), [arXiv:2309.07491].

[363] D. Djukanovic *et al.*, Phys. Rev. D **110**, 1, L011503 (2024), [arXiv:2309.17232].

[364] A. S. Meyer, A. Walker-Loud and C. Wilkinson, Ann. Rev. Nucl. Part. Sci. **72**, 205 (2022), [arXiv:2201.01839].

[365] M. Constantinou *et al.* (2022), [arXiv:2202.07193].

[366] W. Detmold and C. J. D. Lin, Phys. Rev. D **73**, 014501 (2006), [hep-lat/0507007].

[367] A. J. Chambers *et al.*, Phys. Rev. Lett. **118**, 24, 242001 (2017), [arXiv:1703.01153].

[368] A. Shindler, Phys. Rev. D **110**, 5, L051503 (2024), [arXiv:2311.18704].

[369] J. Liang *et al.* (XQCD), Phys. Rev. D **101**, 11, 114503 (2020), [arXiv:1906.05312].

[370] M. Asakawa, T. Hatsuda and Y. Nakahara, Prog. Part. Nucl. Phys. **46**, 459 (2001), [hep-lat/0011040].

[371] A. Rothkopf, J. Comput. Phys. **238**, 106 (2013), [arXiv:1110.6285].

[372] X. Ji, Phys. Rev. Lett. **110**, 262002 (2013), [arXiv:1305.1539].

[373] X. Ji, Sci. China Phys. Mech. Astron. **57**, 1407 (2014), [arXiv:1404.6680].

[374] G. S. Bali *et al.*, Phys. Rev. D **93**, 9, 094515 (2016), [arXiv:1602.05525].

[375] R. Zhang *et al.* (2025), [arXiv:2501.00729].

[376] Y. Zhao, PoS **SPIN2023**, 035 (2024).

[377] S. Bhattacharya, PoS **LATTICE2024**, 013 (2025), [arXiv:2502.00481].

[378] H.-W. Lin, Prog. Part. Nucl. Phys. **144**, 104177 (2025), [arXiv:2506.05025].

[379] Q.-A. Zhang *et al.* (Lattice Parton), Phys. Rev. Lett. **125**, 19, 192001 (2020), [arXiv:2005.14572]; Y. Li *et al.*, Phys. Rev. Lett. **128**, 6, 062002 (2022), [arXiv:2106.13027]; P. Shanahan, M. Wagman and Y. Zhao, Phys. Rev. D **104**, 11, 114502 (2021), [arXiv:2107.11930]; M.-H. Chu *et al.* (Lattice Parton (LPC)), Phys. Rev. D **106**, 3, 034509 (2022), [arXiv:2204.00200]; A. Avkhadiev *et al.*, Phys. Rev. Lett. **132**, 23, 231901 (2024), [arXiv:2402.06725]; D. Bollweg *et al.*, Phys. Lett. B **852**, 138617 (2024), [arXiv:2403.00664].

[380] A. Shindler, PoS **EuroPLEx2023**, 024 (2024).

[381] *Proceedings, 41st International Symposium on Lattice Field Theory*, volume PoS **LATTICE2024** (2024), URL `https://pos.sissa.it/466/`.

[382] A. S. Kronfeld *et al.* (USQCD) (2022), [arXiv:2207.07641]; P. Boyle *et al.*, in "Snowmass 2021," (2022), [arXiv:2204.00039]; D. Boyda *et al.*, in "Snowmass 2021," (2022), [arXiv:2202.05838].

[383] Z. Davoudi *et al.*, in "Snowmass 2021," (2022), [arXiv:2209.10758].

[384] R. C. Brower *et al.* (USQCD), Eur. Phys. J. A **55**, 11, 198 (2019), [arXiv:1904.09964].

[385] C. W. Bauer *et al.*, Nature Rev. Phys. **5**, 7, 420 (2023), [arXiv:2404.06298].